Theoretical Study of Indium Compounds of Interest for Organometallic Chemical Vapor Deposition

ARTICLE *in* THE JOURNAL OF PHYSICAL CHEMISTRY A · FEBRUARY 2000

Impact Factor: 2.69 · DOI: 10.1021/jp0013558 · Source: NTRS

Theoretical Study of Indium Compounds of Interest for Organometallic Chemical Vapor Deposition

B. H. Cardelino,*,† C. E. Moore,‡ C. A. Cardelino,§ D. O. Frazier,‡ and K. J. Bachmann||

Chemistry Department, Box 238, Spelman College, Atlanta, Georgia 30314, Space Science Laboratory, NASA George C. Marshall Space Flight Center, Huntsville, Alabama 35812, School of Earth and Atmospheric Sciences, Georgia Institute of Technology, Atlanta, Georgia 30332, and Department of Materials Science and Engineering, North Carolina State University, Raleigh, North Carolina 27695

Received: April 7, 2000; In Final Form: October 24, 2000

The structural, electronic, and thermochemical properties of indium compounds which are of interest in halide transport and organometallic chemical vapor deposition processes have been studied by ab initio and statistical thermodynamic methods. The compounds reported include: indium halides and hydrides (InF, InCl, $InCl_3$, InH, InH_2, InH_3); indium clusters (In_2, In_3); methylindium, dimethylindium, and their hydrogen derivatives [$In(CH_3)$, $In(CH_3)H$, $In(CH_3)H_2$, $In(CH_3)_2$, $In(CH_3)_2H$]; dimethylindium dimer [$In_2(CH_3)_4$] and trimethylindium [$In(CH_3)_3$]; dehydrogenated methyl-, dimethyl-, and trimethylindium [$In(CH_3)_2CH_2$, $In(CH_3)CH_2$, $In(CH_2)$]; trimethylindium adducts with ammonia, trimethylamine and hydrazine [$(CH_3)_3In{:}NH_3$, $(CH_3)_3In{:}N(CH_3)_3$, $(CH_3)_3In{:}N(H_2)N(H_2)$]; dimethylamino-indium and methylimino-indium [$In(CH_3)_2(NH_2)$, $In(CH_3)(NH)$]; indium nitride and indium nitride dimer (InN, In_2N_2); indium phosphide, -arsenide, and -antimonide (InP, InAs, InSb). The predicted electronic properties are based on density functional theory calculations; the calculated thermodynamic properties are reported following the format of the JANAF (Joint Army, Navy, NASA, Air Force) Tables. Equilibrium compositions at two temperatures (298 and 1000K) have been analyzed for groups of competing simultaneous reactions.

Introduction

There is growing interest in extending organometallic chemical vapor deposition (OMCVD) to III−V materials such as indium nitride (InN) that exhibit large thermal decomposition at their optimum growth temperature.[1] The III−V nitrides are candidate materials for light-emitting diodes and semiconductor lasers operating into the blue and ultraviolet regions.[2] To overcome decomposition of the deposited compound, the reaction must be conducted at high pressures. At high pressures, the decomposition of the source vapors occurs in the vapor phase, which has the advantage of simplifying the surface chemistry. However, to avoid problems of uniformity associated with large Reynolds number flows, current industrial processes focus on OMCVD in the viscous flow regime at subatmospheric pressure.

Because of the high thermal decomposition pressure of InN, OMCVD growth has been limited thus far to gallium-rich alloy compositions. Growth of pure InN at pressures below 1 atm is restricted to temperatures that represent a poor match to the optimum processing temperature for GaN. Epitaxial growth of InN at higher temperatures has been attempted, but at pressures below 1 atm it results in incorporation of indium metal droplets into the InN films.[3,4]

On the basis of stabilization data of the InN surface with regard to thermal decomposition under a blanket of molecular nitrogen at high pressures, InN growth should be possible at substrate temperatures up to 900 K.[2,5] Microgravity may provide the venue for maintaining conditions of laminar flow under high pressure.[6] Since the selection of optimized parameters becomes crucial when performing experiments in microgravity, efforts are presently geared to develop computational OMCVD models that will couple the reactor fluid dynamics with its chemical kinetics.[7]

Moreover, fundamental properties of InN are poorly understood for lack of access to high quality crystals or heteroepitaxial layers of this material.[1] In addition, little information is available regarding gas-phase properties of other indium compounds that may be produced from the source vapors. The lack of knowledge of these properties must be corrected in order to support the development of realistic OMCVD simulations.

A second problem of group III nitride epitaxy is the absence of lattice-matching substrates. Epitaxial films grown on strongly mismatched substrates (like sapphire) suffer from high densities of extended defects that, in applications such as confined heterostructure laser diodes, cause difficulties with both device performance and reliability. Using epitaxial lateral overgrowth of silica-masked sapphire substrates, local regions of low defect density GaN have been attained.[8] However, free-standing doped GaN substrates would be far more attractive, since they would match the thermal expansion behavior of the epitaxial films and allow application of large area back-contacts. Such substrates may become available by thick-film halide transport epitaxy, which provides for the required high growth rate to support production with a reasonable throughput. In the overall transport reaction, GaCl and ammonia may react in the gas phase to form deposits of GaN as well as gaseous hydrogen chloride and molecular hydrogen. Thus, 400 μm thick GaN films have been grown on ZnO buffer layers over sapphire by halide transport.[9]

* To whom correspondence should be addressed. E-mail: cardelino@spelman.edu. Fax: (404) 215-7874.
† Chemistry Department.
‡ Space Science Laboratory.
§ School of Earth and Atmospheric Sciences.
|| Department of Materials Science and Engineering.

10.1021/jp0013558 CCC: $20.00
Published on Web 01/17/2001

But the ZnO buffer layers were very thin, making their removal by etching and lift off usable free-standing GaN films difficult. However, Hasegawa et al.[10] have shown that thick film of GaN can be grown after interlayer growth at 1123 K on GaAs(111), which makes GaN substrate fabrication on an industrial scale likely to emerge in the near future.

In the present paper, we report calculated structural, electronic, and thermodynamic properties for indium compounds that are of interest in halide transport and OMCVD simulations, particularly for group III nitrides. The goal of this work was to obtain a related and consistent set of enthalpies and entropies for indium species that may be used for modeling. To account for electron correlation, our calculations were performed based on density functional theory (DFT), which is a suitable method for relatively large molecules. DFT has been shown to be capable of reliably predicting frequencies, an important property in thermodynamic calculations, for indium dihydride[11] and indium trihydride.[12] It should be noted that our DFT calculations do not include relativistic effects.

Because of the richness in both experimental data and high level calculations with relativistic effects available for indium halides, we have included in our study InF, InCl and $InCl_3$ to evaluate our calculations. Coupled-cluster calculations with relativistic corrections have been performed by Leininger et al.[13] for InF and InCl, and by Bauschlicher[14] and Schwerdtfeger et al.[15] for InCl and $InCl_3$. Nonrelativistic calculations using finite difference Hartree−Fock have been performed by Moncrieff et al.[16] on InF, single-determinant Hartree−Fock calculations for InF and InCl by Dobbs and Hehre,[17] and Møller−Plesset perturbation theory on $InCl_3$ by Okamoto.[18] Also available are heats of atomization for indium fluoride and indium chloride[19] and heats of formation for indium fluoride, chloride, and trichloride.[20,21] Experimental vibrational frequencies have been reported for InF and InCl,[19] as well as for indium trichloride.[22]

In addition to the halides, the species studied are classified under the following categories: *indium hydrides* (InH, InH_2, InH_3); *indium clusters* (In_2, In_3); *indium alkylides and their hydrogen and dehydrogenated derivatives* [$In(CH_3)$, $In(CH_3)H$, $In(CH_3)H_2$, $In(CH_3)_2$, $In(CH_3)_2H$, $In_2(CH_3)_4$, $In(CH_3)_3$, $In(CH_2)$, $In(CH_3)CH_2$, $In(CH_3)_2CH_2$]; *trimethylindium adducts* with ammonia, trimethylamine, hydrazine, and derivatives [$(CH_3)_3In:NH_3$, $(CH_3)_3In:N(CH_3)_3$, $In(CH_3)_2(NH_2)$, $In(CH_3)(NH)$, $(CH_3)_3In:N(H_2)N(H_2)$]; *indium-group V species* (InN, In_2N_2, InP, InAs, InSb).

Several relativistic calculations have been performed for the indium hydrides: configuration-interaction calculations by Teichteil and Spiegelmann[23] on InH; multiconfiguration self-consistent-field by Balasubramanian[24] on InH, and by Balasubramanian and Tao[25] on InH_2 and InH_3; coupled-cluster calculations on InH by Leininger.[13] In addition, nonrelativistic Hartree−Fock calculations on InH and InH_3 were performed by Dobbs and Hehre,[17] coupled-cluster and DFT calculations on InH and InH_2 by Pullumbi et al.,[11] and InH_3 by Pullumbi et al.[12] Both of these two last papers also report vibrational frequencies from infrared-matrix isolation measurements. InH vibrational spectra were analyzed by Bahnmaier et al.[26] and White et al.[27] and also reported by Rosen.[28]

The dissociation energy of In_2 has been measured by Balducci et al.,[29] and multiconfiguration self-consistent-field calculations with relativistic corrections have been performed on indium dimer[30] and indium trimer.[31] Calculations on In_2 using energy-adjusted pseudopotentials have been reported by Igel-Mann et al.;[32] El-Nahas and Schleyer[33] report quasi-relativistic multielectron calculations on $In(CH_3)H_2$. The thermal decomposition of trimethylindium [$In(CH_3)_3$] has been studied by mass spectrometry by Buchan et al.,[34] and electron diffraction and infrared spectroscopy has been performed on the trimethylamine adduct of trimethylindium [$(CH_3)_3In:N(CH_3)_3$] by Bradley et al.[35]

The thermal stability of indium nitride has been studied in films by Ambacher et al.[2] and in single crystals by Krukowski et al.[5] The electronic structure of indium nitride single crystals has been studied by photoelectron spectroscopy by Guo et al.[36] The dissociation energy of InSb has been measured by Balasubramanian.[37] Multiconfiguration self-consistent-field calculations have been performed by Balasubramanian et al.[38] for InSb and by Liao and Balasubramanian[39] for In_2Sb_2.

The next section describes the methodology used to compute the consistent set of thermodynamic parameters for the indium compounds.

Method

Molecular structures, energetics, and vibrational frequencies have been obtained from all-electron calculations, using the quantum mechanical program Gaussian98 (Revision A7).[40] The theoretical approach selected is based on density functional theory (DFT), namely B3LYP, which consists of Becke's three-parameter functionals[41] with Lee−Yang−Parr's correlation functionals.[42,43] The basis sets selected are as follows: standard 3-21 g(d,p) on As, Sb, and In,[44,45,46] augmented with the AKR4[47] extended basis sets, and standard 6−311 g(d,p) on all other atoms. The AKR4 set adds onto the standard set a range of tight to diffuse functions as follows: six s-type basis functions containing 4, 3, 3, 3, 2, and 1 primitive functions; five p-type basis functions containing 4, 3, 3, 2, and 1 primitives, and three d-type basis functions containing 4, 2, and 1 primitives. This selection results in 71 basis functions (13s/11p/5d) and 157 primitives on As, 72 basis functions (12s/10*p*/6d) and 190 primitive functions on Sb and In, 6 basis function (3s/1p) and 8 primitive functions on H, 18 basis functions (4s/3p/1d) and 32 primitive functions on C and N; 26 basis functions (6s/5p/1d) on P and Cl, with 46 and 49 primitive functions, respectively. DFT is a computational method suitable for relatively large molecules.

Because of the flatness of the potential energy surfaces of the indium compounds, we have performed self-consistent-field calculations with initial full accuracy and tight convergence criterion ($<10^{-7}$). The stringency of the geometry optimization convergence criteria (10^{-3} to 10^{-6} for maximum and root-mean-square force as well as displacement) was such that no imaginary vibrational frequencies would show and that the wave function would test stable. The default integration grid was used. Finally, a population analysis was performed to confirm that a correct molecular orbital configuration had been achieved.

Using statistical thermodynamics, we have calculated heat capacities at constant pressure (C_p), enthalpies (H), and entropies (S) for the indium compounds that are of interest in OMCVD. The molecular information on a single-component system is contained in the canonical partition function Q which can be expressed as $(1/N!)\ q^N$, in terms of the molecular partition function q. The latter can then be expressed in terms of its quantum mechanical energy states E_i and degeneracy g_i, as $q = \Sigma_i\ g_i \exp\{-[E_i/(kT)]\}$, where k is the Boltzman constant and T the absolute temperature. In the present calculations, we assumed that the contributions to the energy are independent of each other, such that the molecular energy can be separated in terms of electronic, translational, vibrational, external and internal rotational molecular motions, ($E_{el} + E_{tr} + E_v + E_r +$

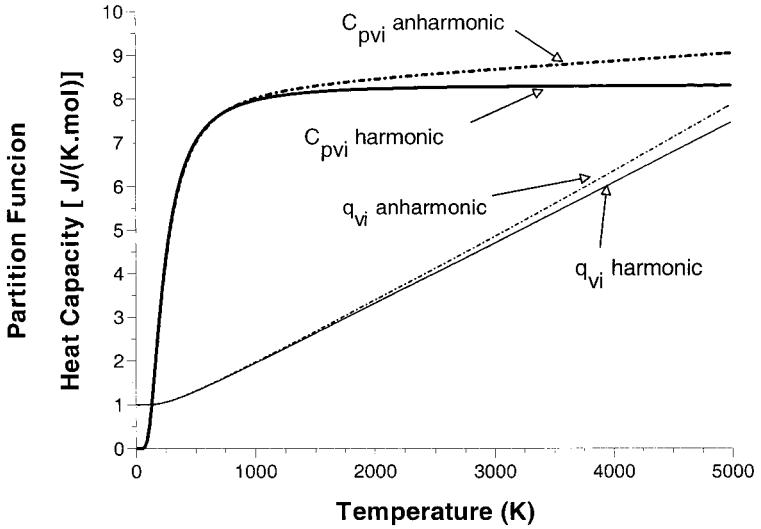

Figure 1. Properties of the In−C asymmetric stretching in $In(CH_3)$. Harmonic and anharmonic partition functions (q_{vi}) are shown as regular solid and dotted lines, respectively; harmonic and anharmonic heat capacities are displayed as bold solid and dotted lines, respectively.

E_{ir}), and that the molecular partition function can be similarly factorized ($q_{el}\ q_{tr}\ q_v\ q_r\ q_{ir}$).

On the basis of classical statistical thermodynamics, and using the zero-point energy (U_0) as the reference value, molar internal energy can be expressed as $U_0 + RT^2\ (\partial \ln Q/\partial\ T)_{V,N}$; molar enthalpy ($H$) as $U + VP$ or $U_0 + RT^2\ (\partial \ln Q/\partial\ T)_{V,N} + VR\ T(\partial \ln Q/\partial\ V)_{T,N}$; molar entropy (S) as $U/T + R \ln Q$; and molar heat capacity at constant pressure (C_p) as $(\partial H/\partial T)_{P,N}$ or $(\partial U/\partial T)_{P,N} + P(\partial V/\partial T)_{P,N}$, where V is the molar volume, P the pressure, and R the gas constant.

Since the zero-point energy is selected as a reference value, the electronic partition function q_{el} is expressed as $g_{el,0} + \Sigma_i\ g_{el,i}\ \exp\{-E_{el,i}/(kT)\}$. Because of the relatively large energy separation between electronic states, q_{el} can usually be assumed to be equal to the degeneracy of the ground state, except at high temperatures. In this work, the expression for q_{el} has been truncated after the first excited state and its energy has been approximated with the HOMO−LUMO (highest occupied and lowest unoccupied molecular orbital) difference. For $In(CH_3)_3$, with multiplicity equal to one, the second term results in a q_{el} of 1.00007 at 6000 K, which corresponds to a contribution to the entropy of 5×10^{-7} kJ mol^{-1}.

The molecular partition function of translation q_{tr} is calculated as a function of temperature and molar volume as $(2\pi MRTh^{-2})^{1.5}\ L^{-4}V$, where M is the molar mass, h is Planck's constant, and L is Avogadro's number. If it is assumed that the equation of state can be approximated as $PV = zRT$, with z being the compressibility factor, the expression for q_{tr} becomes $z\ (2\pi M)^{1.5}(RT)^{2.5}h^{-3}L^{-4}P^{-1}$. The translational molecular partition function is the only partition function that depends on P. In this work, where calculations are restricted to 1 atm, ideality is assumed and z is equal to 1.

Assuming harmonicity, the molecular vibrational partition function q_v is calculated as the product of the $[1 - \exp\{-h\nu_j/(kT)\}]^{-1}$ terms. The parameter j varies from 1 to $3n-5$ in linear molecules and from 1 to $3n-6$ in nonlinear molecules, where n is the number of atoms in the molecule, and ν_j is the harmonic vibrational frequency of the jth vibrational state.

The molecular partition function for external rotation q_r is calculated assuming the rigid rotor approximation which is valid when T is much greater than $h^2/(8\pi^2 Ik)$ (where I is an average moment of inertia for the molecule). The expression of q_r for linear molecules is $(8\pi^2 IkT)/h^2$, and for nonlinear molecules is $(\pi^{1/2}/\sigma_r)[(8\pi^2 kT)/h^2]^{3/2}\ (I_A I_B I_C)^{1/2}$, where I_A, I_B, I_C are the moments of inertia in the three directions and σ_r is the symmetry number of the external rotation.

Assuming free internal rotations, the corresponding molecular partition function q_{ir} is calculated as $(1/\sigma_{ir})(8\pi^3 I_{rir} k\ T/h^2)^{1/2}$, where σ_{ir} is the symmetry number of the internal rotation. The reduced moment of inertia of the rotating group I_{rir} is obtained from: $I_{ir}\ [1 - I_{ir}\ (\cos^2 \alpha/I_A + \cos^2 \beta/I_B + \cos^2 \gamma/I_C)]$, where I_{ir} is the moment of inertia of the rotating group with respect to the axis of internal rotation, and α, β and γ are the angles of the corresponding principal axes with the axis of internal rotation. When the molecule has more than one rotating group, it is assumed that q_{ir} is a product of the individual internal rotation partition functions. To avoid double counting, the vibrational frequency (ν) corresponding to each internal rotation is eliminated. Its value is estimated from its rotational barrier ($u_{ir,max}$) and the potential energy relationship $^1/_2 h\nu = {}^1/_2 u_{ir,max}\ (1 - \cos n\phi)$, where n is the number of maxima in a complete rotation and ϕ is the angle between the axis of rotation and the outer atom (or atoms) of the rotating group. A hindered rotation is assumed to occur when the inverse of the internal partition function ($1/q_{ir}$) is smaller than 0.95 and the rotational barrier divided by kT($u_{ir,max}/kT$) is less than 20. In the case of a hindered rotation, its contributions to the thermodynamic properties are evaluated using the tables provided by Lucas.[48] These tables have been obtained from quantum mechanical calculations and are reported as a function of $1/q_{ir}$ and $u_{ir,max}/kT$. The importance of internal rotations in the calculations can be shown in the case of $In(CH_3)_3$, with three rotating groups. Our calculations show that the heat capacity at 100 K rises from 79 to 92 J K^{-1} mol^{-1} (16%) when the contribution from internal rotations are included, but the percent change drops with increasing temperature and at 1000 K the heat capacity rises from 225 to 238 J K^{-1} mol^{-1} (6%).

The above expressions for q_v and q_r are based on the rigid rotator-harmonic oscillator model, to which a contribution from internal rotations (q_{ir}) is added. In this model, the interatomic distances are considered fixed, the intramolecular potential energy is approximated by a parabolic function, and the molecular rotation and vibration are considered to be independent of each other. At higher temperatures, faster rotations make the molecule stretch and increase its moment of inertia. Similarly, in strong vibrations it becomes apparent that the

potential energy deviates from a simple parabola, and the distance between two atoms increases due to the anharmonicity of the potential function. Consequently, the intermolecular distance becomes a function of the vibrational state leading to coupling between rotation and vibration.[48]

To roughly estimate the effect of anharmonicity, we consider the vibration leading to dissociation of a methyl group from $In(CH_3)$, with a harmonic frequency ν_0 of 500 cm^{-1}. Using the classical Morse potential energy function $D_e[1 - \exp\{-(\alpha/R_e)-(R - R_e)\}]^2$ (where R is the In−C distance and R_e its equilibrium value of 2.25 Å, and D_e the dissociation energy), one can estimate the anharmonicity constant x_e from $(\alpha/R_e)^2h/(8\pi^2\mu\nu_0)$, where μ is the reduced mass of the two separating sections. On the basis of DFT energies obtained from a relaxed scanning between 2.20 and 2.65 Å for the In−C bond and fitting the data into a polynomial, we obtain x_e equal to 3.876×10^{-3}. Figure 1 shows the calculated harmonic and anharmonic values for the partition function q_{vi} and the heat capacity corresponding to that particular vibration. At 300 K, anharmonicity increases the heat capacity by 0.053 J K^{-1} mol^{-1}, which corresponds to an increase of 1% in the heat capacity corresponding to that vibration and 0.3% in the total vibrational heat capacity of the molecule. At 1000 K, the increase is by 0.049 J K^{-1} mol^{-1}, and the percentages become 0.6% and 0.1%, respectively; while at 5000 K, the increase is by 0.74 J K^{-1} mol^{-1}, corresponding to 8% for that particular vibration and 1% to the total vibrational heat capacity. The changes in percentages are due to the general shape of the vibrational heat capacity curve coupled to the increase of the anharmonicity effect with temperature. The example seems to suggest that anharmonicity effects become significant only at very high temperatures. In our calculations we have not included the anharmonicity effect.

The calculations of C_p, H, and S for the indium compounds were performed for temperatures between 10 and 6000 K and then the resulting values were fitted to temperature following the format of the JANAF (Joint Army, Navy, NASA, Air Force) Tables.[49] However, we used a different base for enthalpy and entropy. We have similarly obtained 14 coefficients to estimate the thermodynamic properties at standard atmospheric pressure for two temperature ranges (300−1000 K and 1000−5000 K). The seven coefficients (z_1 to z_7) of each set satisfy the following equations:

$$C_p/R = z_1 + z_2T + z_3T^2 + z_4T^3 + z_5T^4 \quad (1)$$

$$H/R = z_1T + (z_2/2)T^2 + (z_3/3)T^3 + (z_4/4)T^4 + (z_5/5)T^5 + z_6 \quad (2)$$

$$S/R = z_1 \ln T + z_2T + (z_3/2)T^2 + (z_4/3)T^3 + (z_5/4)T^4 + z_7 \quad (3)$$

where R is the universal gas constant, T is temperature in Kelvin, and C_p is defined as $(\partial H/\partial T)_P$. In the present work, enthalpies and entropies are based on direct quantum/statistical thermodynamic calculations. In the JANAF tables, enthalpies are defined in terms of standard heats of formation (H^0_f) from elements in their reference states, and entropies in terms of third-law entropies (S^0_{3-law}), as shown in eqs 4 and 5:

$$H_{hof} = H^0_f + \int_{298}^{T} C_p \, dT \quad (4)$$

$$S_{3-law} = S^0_{3-law} \int_{298}^{T} (C_p/T) \, dT \quad (5)$$

The choice of a different reference value results in different z_6 and z_7 coefficients for enthalpy and entropy, respectively, which are the temperature independent terms in eqs 2 and 3. Theoretically, these coefficients correspond to

$$z_6 = (\text{DFT electronic energy} + \text{zero-point energy})/R \quad (6)$$

$$z_7 = A + \ln(q_e) + \ln(q_t/T^{5/2}) + \ln(q_r/B) \quad (7)$$

where $A = 3.5$ and $B = T$ for linear molecules and $A = 4$ and $B = T^{3/2}$ for nonlinear molecules. Equation 7 contains the temperature-independent terms from $(U - U_0)/T$ and the temperature-independent portions of the electronic (q_e), translational (q_t), and rotational (q_r) partition functions, resulting from the properties of logarithms. U corresponds to the internal energy and U_0 to the DFT electronic energy with the zero-point energy correction.

On the other hand, in eqs 4 and 5,

$$z_6 = H^0_f/R - \sum_{n=1}^{5} z_n x 298.15^n/n \quad (8)$$

$$z_7 = S^0_{3-law}/R - z_1 \ln(298.15) - \sum_{n=2}^{5} z_n x 298.15^{n-1}/(n-1) \quad (9)$$

Finally, the theoretical temperature-independent term z_1 of eq 1 is equal to 3.5 for a linear molecule or 4 for a nonlinear molecule.

A FORTRAN program[50] has been written to calculate C_p, S, and H for temperatures between 10 and 6000 K, in increments of 1 K, using statistical thermodynamics. The C_p values are used to obtain the z_1 to z_5 coefficients of eq 1. Values between 10 and 2000 K are used to obtain the fitting coefficients for the first temperature range (100−1000 K), whereas values between 800 and 6000 K are used for the second temperature range (1000−5000 K). z_6 from eq 6 and z_7 from eqs 3 and 7 are determined as the average difference between the statistical thermodynamic temperature-dependent part of H/R and S/R, respectively, and the time-dependent values obtained using the z_1 to z_5 coefficients from the C_p/R expansion.

As an example to show the quality of the equation fitting, we use trimethylindium [$In(CH_3)_3$]. Figure 2 displays the fitted and statistical thermodynamic values of C_p, S, and the temper-

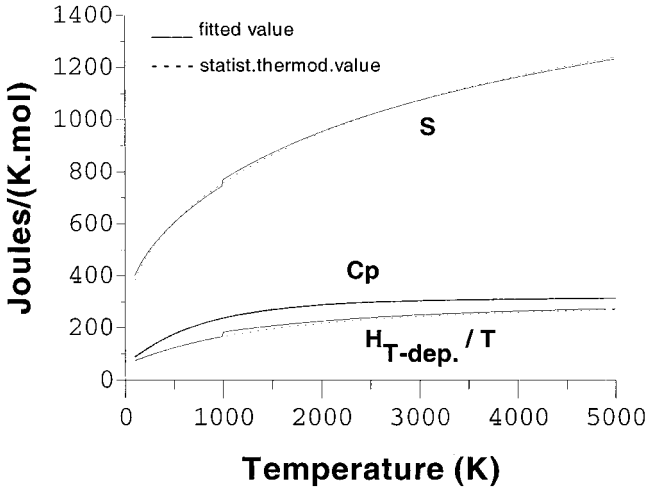

Figure 2. Entropy (S), heat capacity at constant pressure (C_p), and the time-dependent component of enthalpy for trimethylindium as a function of temperature, from DFT and statistical thermodynamic calculations. The dotted line corresponds to a curve fit.

TABLE 1: Calculated Properties for In(CH_3), in and CH_3 Using Different DFT Functionals and Basis Sets

functional	basis set on In	basis set on CH_3	In−C distance å	In−CH_3 harmonic frequency cm^{-1}	standard enthalpy (hartree)	standard enthalpy (kJ mol^{-1})
		In(CH_3) Calculations				
B3LYP	3-21G(d,p) AKR4 72 basis functions 190 primitive functions	6-311G(d,p) 36 basis functions 56 primitive functions	2.269	499.6	−5778.579232	
B3LYP	3-21G(d,p) AKR4	6-311++G(d,p) 43 basis functions 63 primitive functions	2.262	491.1	−5778.582500	
B3P86	3-21G(d,p) AKR4	6-311G(d,p)	2.245	501.5	−5779.986272	
B3PW91	3-21G(d,p) AKR4	6-311G(d,p)	2.251	503.3	−5778.630281	
BHandHLYP	3-21G(d,p) AKR4	6-311G(d,p)	2.246	522.2	−5778.522657	
		In Calculations				
B3LYP	3-21G(d,p) AKR4				−5738.673344	
B3P86	3-21G(d,p) AKR4				−5739.915755	
B3PW91	3-21G(d,p) AKR4				−5738.740031	
BHandHLYP	3-21G(d,p) AKR4				−5738.652492	
		CH_3 Calculations				
B3LYP		6-311G(d,p)			−39.820157	
B3LYP		6-311++G(d,p)			−39.821546	
B3P86		6-311G(d,p)			−39.979995	
B3PW91		6-311G(d,p)			−39.803458	
BHandHLYP		6-311G(d,p)			−39.789652	
		In(CH_3) → In + (CH_3) Calculations				
B3LYP		6-311G(d,p)			0.085731	225.09
B3LYP		6-311++G(d,p)			0.087610	230.02
B3P86		6-311G(d,p)			0.090522	237.67
B3PW91		6-311G(d,p)			0.086792	227.87
BHandHLYP		6-311G(d,p)			0.080513	211.39

ature-dependent component of H (H_{T-dep}) divided by T, respectively. The theoretical temperature-independent term (z_1) for trimethylindium should be 4. The values obtained for z_1 from the C_p/R fits were 7.3 at the lower temperature range and 13.9 at the higher range. The small difference between the fitted and statistical thermodynamic values of H_{T-dep} is a consequence of the difference between the theoretical and fitted z_1 values. This error is incorporated into the calculation of z_6, thus resulting in a perfect match between the fitted and the statistical mechanics values of H.

In addition, a comparison for In(CH_3), In, and (CH_3) was performed using four different DFT methods and two different basis sets. The DFT methods considered are B3LYP,[41,42,43] B3P86,[51] B3PW91,[52] and BHandHLYP,[40] with different hybrid correlation functions of the electron density (functionals). The basis sets used correspond to the one previously discussed for In [3-21G(d,p) augmented with AKR4] and for the other atoms [6-311G(d,p)], and the addition of diffuse functions for C and H atoms [6-311++G(d,p)]. The basis set on the In atom was kept unchanged, since it is the best available choice within Gaussian98.[40] The results from the comparisons are summarized in Table 1. The properties compared are the In−C distance, the harmonic stretching frequency for the In−C bond, the standard enthalpy for the three species, and the enthalpy for the dissociation of In(CH3) into In atom plus methyl radical.

The two B3LYP calculations result on the larger In−C bond distances, but all bond distances are within 1%. Addition of diffuse functions drops the In−C stretching frequency by 8 cm^{-1}, about 1.7%. B3LYP, B3P86, and B3PW91 give this frequency within less than 1% while BHandHLYP results in a frequency 4.5% higher. To exemplify how the differences in energy and frequency propagate into the calculation of the thermodynamic properties, Table 1 contains the standard enthalpy of dissociation for singlet In(CH_3) into doublet In and doublet CH_3. The standard enthalpies of dissociation values are very close for the first three DFT methods (within 2%). Addition of the diffuse functions on C and H results on a drop of 2% in the standard enthalpy of dissociation, close to the value obtained with B3PW91 without the diffuse functions.

Results

The DFT calculated data obtained for the indium species studied are contained in Tables 2 through 4 and Table 8, Appendix 1. The DFT electronic energy and the zero-point correction for all of the species studied are shown in Table 2. Several points must be made with respect to the table: (a) all available significant figures have been included to allow for subtraction of large similar numbers, even though the precision of the calculations would justify no more than three decimal places in total energy; (b) the energy unit shown is hartree per particle, which should be multiplied by 2625.5 to obtain Joules per mole or 627.51 for kcal per mole; (c) energies for species that do not contain indium but that are required in some derived calculations, such as dissociation energies or equilibrium compositions, have been calculated at the same level of approximation as the indium species; (d) the zero-point corrections are calculated as half the sum of the harmonic frequencies.

Table 3 summarizes the unique structural parameters that describe each species studied. Table 4 contains the uncorrected vibrational frequencies. There is evidence that DFT vibrational frequencies and zero-point corrections should be multiplied by factors between 0.96 and 1.01[53,54] depending on the basis set used. We preferred not to include any correction until systematic errors for DFT calculations on indium compounds are better known. The coefficients obtained for the calculation of heat capacities, entropies and enthalpies between 100 and 5000 K based on eqs 1−3 are contained in Table 8, Appendix 1.

Enthalpies of dissociation reactions important for OMCVD modeling are contained in Table 5, at 0, 298.15, and 1000K. These values have been obtained from the data reported in Table

TABLE 2: DFT Energy and Zero-point Correction for Indium Species[a]

species	point group	state	DFT energy	zero-point correction
		Indium Halides		
InF	$C_{\infty v}$	$^1\Sigma^+$	−5838.63087536	0.001255
InCl	$C_{\infty v}$	$^1\Sigma^+$	−6199.00630492	0.000684
$InCl_3$	D_{3h}	$1A_1'$	−7119.53625006	0.003077
		Indium Clusters		
In doublet	K_H	$^2P_{1/2}$	−5738.67570450	0.000000
In quartet	K_H	$^4P_{5/2}$	−5738.52422795	0.000000
In_2 triplet	$D_{\infty h}$	$^3\pi_u$	−11477.3978308	0.000244
In_2 quintet	$D_{\infty h}$	$^5\Sigma_u$	−11477.3077073	0.000464
In_3 quartet	C_{2v}	$^4A_2$	−17216.1301029	0.000662
In_3 quartet	$D_{\infty h}$	$^4\Sigma_u^-$	−17216.1271044	0.000802
		Indium Hydrides		
InH singlet	$C_{\infty v}$	$^1\Sigma$	−5739.27972049	0.003285
InH triplet	$C_{\infty v}$	$^3\pi$	−5739.20628131	0.003378
InH_2	C_{2v}	$^2A_1$	−5739.84350262	0.008869
InH_3	D_{3h}	$^1A_1'$	−5740.46386640	0.016190
		Indium Alkylides		
$In(CH_3)$ singlet	C_{3v}	$^1A_1$	−5778.61703748	0.033257
$In(CH_3)$ triplet	C_s	$^3A'$	−5778.54520911	0.033949
$In(CH_2)$	C_{2v}	$^2A_1$	−5777.94951736	0.019939
$In(CH_3)H$	C_s	$^2A'$	−5779.18009109	0.038981
$In(CH_3)H_2$	C_s	$^1A'$	−5779.79945314	0.046104
$In(CH_3)_2$	C_2	^2A	−5818.51601142	0.068798
$In(CH_3)(CH_2)$ singlet	C_1	^1A	−5817.86591503	0.057236
$In(CH_3)(CH_2)$ triplet	C_1	^3A	−5817.84649508	0.056169
$In_2(CH_3)_4$	D_2	^1A	−11637.1153789	0.140335
$In(CH_3)_2H$ quasi-C_s	C_1	^1A	−5819.13461615	0.074611
$In(CH_3)_2H$ quasi-C_{2v}	C_2	^1A	−5819.11581121	0.073509
$In(CH_3)_3$	C_{3v}	$^1A_1$	−5858.46910188	0.104916
$In(CH_3)_2(CH_2)$	C_1	^2A	−5857.79968389	0.092015
		Trimethylindium Adducts and Derivatives		
$(CH_3)_3In{:}NH_3$	C_{3v}	$^1A_1$	−5915.07447231	0.142531
$(CH_3)_2InNH_2$	C_2	^1A	−5874.53406226	0.094816
$(CH_3)InNH$ singlet	C_1	^1A	−5833.93275002	0.047319
$(CH_3)InNH$ triplet	C_1	^3A	−5833.89990026	0.045203
$(CH_3)_3In{:}N(CH_3)_3$	C_{3v}	$^1A_1$	−6033.02120632	0.227299
$(CH_3)_3In{:}N(H_2)N(H_2)$	C_1	^1A	−5970.39948316	0.160937
		Indium - Group V		
InN	$C_{\infty v}$	$^3\Sigma^-$	−5793.34006937	0.001360
In_2N_2 linear	$D_{\infty h}$	$^3\Sigma_g$	−11586.9343483	0.006790
In_2N_2 rhombic	D_{2h}	^1A_g	−11586.9331871	0.006434
InP	$C_{\infty v}$	$^3\Sigma^-$	−6080.02744457	0.000540
InAs	$C_{\infty v}$	$^3\Sigma^-$	−7974.57555548	0.000394
InSb	$C_{\infty v}$	$^3\Sigma^-$	−12050.4658980	0.000319
		Other Atoms and Molecules		
H	K_H	$^2S_{1/2}$	−0.502155930036	0.000000
H_2	$D_{\infty h}$	$^1\Sigma_g$	−1.17957102281	0.010068
CH_3	D_{3h}	$^2A_2$"	−39.8537575439	0.029575
CH_4	T_d	$^1A_1$	−40.5337483093	0.044601
C_2H_6	D_{3d}	$^1A_{1g}$	−79.8562599299	0.074376
F	K_H	$^2P_{3/2}$	−99.7538096003	0.000000
Cl	K_H	$^2P_{3/2}$	−460.166160487	0.000000
Cl_2	$D_{\infty h}$	$^1\Sigma_g$	−920.405675822	0.001156
N	K_H	$^4S_{3/2}$	−54.5985431427	0.000000
N_2	$D_{\infty h}$	$^1\Sigma_g$	−109.555930156	0.005576
NH_3	C_{3v}	$^1A_1$	−56.5760352520	0.034295
$N(CH_3)_3$	C_{3v}	$^1A_1$	−174.524485576	0.119643
N_2H_4	C_2	^1A	−111.901535786	0.053279
P	K_H	$^4S_{3/2}$	−341.280503655	0.000000
PH_3	C_{3v}	$^1A_1$	−343.172847759	0.023880
As	K_H	$^4S_{3/2}$	−2235.82983984	0.000000
Sb	K_H	$^4S_{3/2}$	−6311.72500554	0.000000

[a] Units of energy: hartree.

2 and Table 8, Appendix 1 (using eqs 2 and 3). Finally, groups of reactions were organized to evaluate their equilibrium composition at two different temperatures (298.15 and 1000 K), based on Gibbs free energy calculations obtained from the data of Table 8, Appendix 1 (assuming all components in the gas phase). These systems of equations include the pertinent reactions and mass balance equations. The results are summarized in Table 6.

Indium Halides. To evaluate the quality of the computational procedure chosen, we have performed calculations on InCl, $InCl_3$, and InF. We have chosen three properties for comparison with reported data: energy, bond distance, and frequency. Table

TABLE 3: Structural Parameters of Indium Species Based on DFT Calculations[a]

species	point group	state	distances	angles
			Indium Clusters	
InF	$C_{\infty v}$	$^1\Sigma^+$	In−F 2.020	
InCl	$C_{\infty v}$	$^1\Sigma^+$	In−Cl 2.471	
$InCl_3$	D_{3h}	$1A_1'$	In−Cl 2.347(3)	
			Indium Clusters	
In_2 triplet	$D_{\infty h}$	$^3\pi_u$	In−In 3.076	
In_2 quintet	$D_{\infty h}$	$^5\Sigma_u$	In−In 2.658	
In_3	C_{2v}	$^4A_2$	In−In 2.948(2);3.566	unique In−In−In 74
In_3	$D_{\infty h}$	$^4\Sigma_u^-$	In−In 2.875	
			Indium Hydrides	
InH singlet	$C_{\infty v}$	$^1\Sigma$	In−H 1.878	
InH triplet	$C_{\infty v}$	$^3\pi$	In−H 1.813	
InH_2	C_{2v}	$^2A_1$	In−H 1.799(2)	H−In−H 119
InH_3	D_{3h}	$^1A_1'$	In−H 1.766(3)	
			Indium Alkylides	
$In(CH_3)$ singlet	C_{3v}	$^1A_1$	In−C 2.269;C-H 1.096(3)	In−C−H 111(3);H−C−H 108(3)
$In(CH_3)$ triplet	C_s	$^3A'$	In−C 2.365;C-H 1.086(3)	In−C−H 104(3);H−C−H 113(3)
$In(CH_2)$	C_{2v}	$^2A_1$	In−C 2.238;C−H 1.095(2)	In−C−H 125(2);H−C−H 110
$In(CH_3)H$	C_s	$^2A'$	In−C 2.231;In−H 1.811; C−H 1.089;1.093(2)	In−C−H 112; 108(2);H−In−C 118; H−C−H 109;110(3)
$In(CH_3)H_2$	C_s	$^1A'$	In−C 2.195;In−H 1.773(2); C−H 1.094;1.091(2)	H−In−C 121(2);H−In−H 119; H−C−H 109;108(2)
$In(CH_3)_2$	C_2	^2A	In−C 2.242(2); C−H 1.089(2),1.094(4)	C−In−C 117;In−C−H 112(2);108(4); H−C−H 109(4),110(2)
$In(CH_3)(CH_2)$ singlet	C_1	^1A	In−C(CH_3) 2.165;In−C(CH_2) 2.020; C−H(CH_3) 1.091(2),1.090, C−H(CH_2) 1.090(2)	C−In−C 164;H−C(CH_3)−H 109(2),112; H−C(CH_2)−H 115
$In(CH_3)(CH_2)$ triplet	C_1	^3A	In−C(CH_3) 2.238;In−C(CH_2) 2.198; C−H(CH_3) 1.093,1.089,1.093; C−H(CH_2) 1.092,1.089	C−In−C 117;H−C(CH_3)−H 110(2),109; H−C(CH_2)-H 113
$In_2(CH_3)_4$	D_2	^1A	In−In 2.847; In−C 2.218(4); C−H 1.092(4); 1.093(8)	In−In−C 123(4);C−In−C 115(2)
$In(CH_3)_2H$ quasi-C_s	C_1	^1A	In−C 2.200(2);In−H 1.781; C−H 1.091(2);1.093(4)	C−In−C 123;H−In−C 118(2); H−C−H 109(2),110(2),112(2)
$In(CH_3)_2H$ quasi-C_{2v}	C_2	^1A	In−C 2.200(2);In−H 1.781; C−H 1.158(2),1.172(2), 1.170(2)	C−In−C 123;H−In−C 118(2); H−C−H 109(2),110(2),111(2)
$In(CH_3)_3$	C_{3v}	$^1A_1$	In−C 2.208(3);C−H 1.094(3);1.092(6)	In−C−H 109(3);111(6); H−C−H 109(3);108(6)
$In(CH_3)_2(CH_2)$	C_1	^2A	In−C 2.203(2),2.171; C(CH_3)−H 1.091(2),1.092(2), 1.093(2); C(CH_2)-H 1.089(2)	C−In−C 122,119(2); H−C(CH_3)−H 108(2),109(4); H−C(CH_2)−H 112;C−In−C−C 180
			Trimethylindium Adducts and Derivatives	
$(CH_3)_3In{:}NH_3$	C_{3v}	$^1A_1$	In−C 2.223(3);In−N 2.450; C−H 1.093(3);1.094(6);N−H 1.016(3)	C−In−C 119(3);C−In−N 96(3); H−C−In 111(9);H−N−In 120(3)
$(CH_3)_2InNH_2$	C_2	^1A	In−C 2.196(2);In−N 2.058; C−H 1.091(4),1.092(2); N−H 1.010(2)	C−In−C 131(3);C−In−N 115; H−C−H 108(3),109(6);H−N−H 110
$(CH_3)InNH$ singlet	C_1	^1A	In−C 2.152;In−N 1.934; C−H 1.091;1.090(2); N−H 1.024	C−In−N 170;H−C−In 108, 111(2); H−N−In 113(2);H−N−In−C 180
$(CH_3)InNH$ triplet	C_1	^3A	In−C 2.242;In−N 2.192; C−H 1.089;1.093(2);N−H 1.031	C−In−N 110;H−C−In 112, 108(2); H−N−In 112(2);H−N−In−C 180
$(CH_3)_3In{:}N(CH_3)_3$	C_{3v}	$^1A_1$	In−C 2.226(3);In−N 2.476;C(In)−H 1.094(3);1.093(6); N−C 1.475(3);C(N)−H 1.091(6);1.100(3)	C−In−C 118(3);N−In−C 98(3); C−N−C 110(3);H−C−In 110(3);112(6); C−N−In 109(3);H−C−N 111(3);110(6)
$(CH_3)_3In{:}N(H_2)N(H_2)$	C_1	^1A	In−C 2.227,2.225,2.218;In−N 2.453; C(In)−H 1.095,1.094(3);1.093(5); N−N 1.437;N(In)-H 1.020,1.016; N(N)−H 1.015(2)	C−In−C 118;120(2);N−In−C 94,95,98; H−N−H 110(3);H−C−In 110; 111(7);112;In−N−N 114; In−N−H 106,107;N−N−H 107,111
			Indium - Group V	
InN	$C_{\infty v}$	$^3\Sigma^-$	In−N 2.100	
In_2N_2 linear	$D_{\infty h}$	$^3\Sigma_g$	In−N 2.251(2);N−N 1.171	
In_2N_2 rhombic	D_{2h}	^1A_g	In−N 2.400(4);N−N 1.225	In−N−In 150;N−In−N 30
InP	$C_{\infty v}$	$^3\Sigma^-$	In−P 2.696	
InAs	$C_{\infty v}$	$^3\Sigma^-$	In−As 2.775	
InSb	$C_{\infty v}$	$^3\Sigma^-$	In−Sb 2.997	

[a] Units of length: angstrom. Units of angle: degree. Number of instances other than one is shown in parentheses.

7 summarizes the data for InCl and $InCl_3$. Even though we use joules per mole throughout this paper as our preferred energy unit, for the indium halides we use kilocalories per mole, to facilitate comparison with most of the reported data.

Using the DFT energies of Table 2, the computed atomization energy at 0 K (D_0) for singlet InCl (see Table 5, reaction 1) is 103.1 kcal mol^{-1}. Huber and Herzberg[19] report an experimental value of 102.4 kcal mol^{-1} for InCl. In addition, using the

TABLE 4: Vibrational Frequencies of Indium Species Based on DFT Calculations[a]

species	point group	state	vibrational frequencies
			Indium Halides
InF	$C_{\infty v}$	$^1\Sigma^+$	551
InCl	$C_{\infty v}$	$^1\Sigma^+$	300
$InCl_3$	D_{3h}	$^1A_1'$	84, 84, 90, 332, 381, 381
			Indium Clusters
In_2 triplet	$D_{\infty h}$	$^3\pi_u$	107
In_2 quintet	$D_{\infty h}$	$^5\Sigma_u$	204
In_3	C_{2v}	$^4A_2$	42, 121, 128
In_3	$D_{\infty h}$	$^4\Sigma_u^-$	45,45,97,165
			Indium Hydrides
InH singlet	$C_{\infty v}$	$^1\Sigma$	1442
InH triplet	$C_{\infty v}$	$^3\pi$	1483
InH_2	C_{2v}	$^2A_1$	612, 1615, 1666
InH_3	D_{3h}	$^1A_1'$	602, 608, 608, 1761, 1761, 1766
			Indium Alkylides
$In(CH_3)$ singlet	C_{3v}	$^1A_1$	418, 500, 500, 1174, 1445, 1445, 2986, 3066, 3066
$In(CH_3)$ triplet	C_s	$^3A'$	301, 602, 654, 1029, 1421, 1423, 3067, 3192, 3212
$In(CH_3)H$	C_s	$^2A'$	32, 375, 444, 599, 716, 1162, 1444, 1457, 1611, 3025, 3106, 3142
$In(CH_2)$	C_{2v}	$^2A_1$	380, 426, 463, 1354, 3022, 3107
$In(CH_3)H_2$	C_s	$^1A'$	45, 327, 449, 491, 613, 698, 738, 1215, 1460, 1463, 1734, 1741, 3030, 3104, 3129
$In(CH_3)_2$	C_2	^2A	19, 44, 111, 426, 449, 587, 596, 621, 722, 1143, 1169, 1443, 1445, 1453, 1462, 3019, 3021, 3099, 3100, 3135, 3136
$In(CH_3)(CH_2)$ singlet	C_1	^1A	1, 112, 184, 461, 532, 664, 669, 708, 770, 1228, 1350, 1443, 1456, 3041, 3075, 3124, 3138, 3167
$In(CH_3)(CH_2)$ triplet	C_1	^3A	22, 109, 218, 434, 497, 547, 585, 635, 698, 1155, 1344, 1444, 1458, 3025, 3065, 3107, 3140, 3173
$In_2(CH_3)_4$	D_2	^1A	37, 52, 52, 65, 65, 69, 70, 111, 112, 117, 117, 150, 461, 469, 479, 479, 596, 604, 653, 653, 676, 676, 716, 735, 1193, 1193, 1197, 1200, 1456, 1456, 1458, 1460, 1462, 1462, 1462, 1462, 3021, 3022, 3022, 3022, 3096, 3096, 3097, 3097, 3114, 3114, 3114, 3114
$In(CH_3)_2H$ quasi-C_s	C_1	^1A	5, 28, 105, 330, 451, 475, 501, 622, 715, 715, 735, 1209, 1212, 1457, 1460, 1461, 1465, 1717, 3028, 3029, 3100, 3101, 3123, 3123
$In(CH_3)_2H$ quasi-C_{2v}	C_2	^1A	168, 354, 477, 478, 511, 647, 696, 895, 939, 949, 972, 1319, 1321, 1504, 1506, 1510, 1510, 1716, 2408, 2409, 2449, 2449, 2541, 2542
$In(CH_3)_3$	C_{3v}	$^1A_1$	27, 35, 35, 111, 111, 120, 461, 488, 488, 618, 618, 641, 714, 734, 734, 1205, 1205, 1211, 1457, 1459, 1459, 1463, 1463, 1471, 3024, 3024, 3026, 3097, 3097, 3098, 3118, 3119, 3119
$In(CH_3)_2(CH_2)$	C_1	^2A	30, 34, 103, 104, 124, 175, 472, 495, 531, 568, 587, 640, 690, 697, 739, 1208, 1211, 1373, 1459, 1460, 1463, 1468, 3029, 3030, 3080, 3102, 3102, 3122, 3122, 3173
			Trimethylindium Adducts and Derivatives
$(CH_3)_3In{:}NH_3$	C_{3v}	$^1A_1$	49, 70, 70, 76, 87, 87, 104, 104, 119, 255, 455, 458, 458, 482, 482, 618, 641, 641, 692, 713, 713, 1156, 1201, 1201, 1205, 1461, 1461, 1467, 1469, 1471, 1471, 1670, 1670, 3013, 3013, 3015, 3088, 3088, 3088, 3092, 3092, 3092, 3473, 3593, 3593
$(CH_3)_2InNH_2$	C_2	^1A	34, 44, 95, 107, 109, 242, 366, 473, 506, 592, 616, 669, 708, 716, 744, 1209, 1212, 1460, 1462, 1464, 1467, 1554, 3035, 3036, 3114, 3114, 3124, 3124, 3563, 3662
$(CH_3)InNH_2$ singlet	C_1	^1A	46, 154, 204, 503, 682, 719, 740, 811, 1234, 1445, 1451, 3046, 3135, 3145, 3455
$(CH_3)InNH_2$ triplet	C_1	^3A	27, 117, 178, 421, 449, 602, 635, 724, 1146, 1441, 1452, 3026, 3111, 3141, 3373
$(CH_3)_3In{:}N(CH_3)_3$	C_{3v}	$^1A_1$	15, 64, 64, 99, 99, 104, 120, 120, 133, 151, 167, 167, 247, 288, 288, 423, 423, 450, 457, 472, 472, 605, 621, 621, 688, 699, 699, 825, 1027, 1027, 1069, 1122, 1122, 1195, 1195, 1198, 1241, 1283, 1283, 1443, 1443, 1462, 1462, 1465, 1466, 1470, 1470, 1486, 1492, 1495, 1495, 1516, 1516, 1518, 2981, 2981, 2989, 3017, 3017, 3019, 3089, 3089, 3091, 3091, 3092, 3093, 3095, 3096, 3096, 3128, 3132, 3132
$(CH_3)_3In{:}N(H_2)N(H_2)$	C_1	^1A	40, 69, 70, 88, 91, 107, 108, 117, 126, 166, 253, 284, 454, 472, 478, 554, 616, 624, 651, 692, 716, 719, 878, 1080, 1123, 1202, 1203, 1207, 1303, 1361, 1462, 1464, 1468, 1471, 1471, 1475, 1675, 1696, 3010, 3013, 3019, 3082, 3086, 3093, 3093, 3095, 3098, 3438, 3475, 3539, 3568
InN	$C_{\infty v}$	$^3\Sigma^-$	597
In_2N_2 linear	$D_{\infty h}$	$^3\Sigma_g$	69, 69, 115, 298, 298, 388, 1744
In_2N_2 rhombic	D_{2h}	^1A_g	125, 129, 131, 420, 490, 1529
InP	$C_{\infty v}$	$^3\Sigma^-$	237
InAs	$C_{\infty v}$	$^3\Sigma^-$	173
InSb	$C_{\infty v}$	$^3\Sigma^-$	140

[a] Units in cm^{-1}.

experimental heat of formation for InCl from Barin,[20] and after performing a correction from 298 to 0 K for the dissociation of Cl_2, Bauschlicher[14] obtains a D_0 of 103.5 kcal mol^{-1} for InCl. Bauschlicher's[14] all-electron and effective-core-potential coupled-cluster calculations (extrapolated to the complete basis set limit) for InCl result in 109.1 and 108.6 kcal mol^{-1}, respectively, before relativistic corrections, and 102.8 and 103.5 kcal mol^{-1}, respectively, after these corrections. Schwerdtfeger et al.[15] coupled-cluster calculations with relativistic pseudopotentials result in values ranging from 102.8 to 97.3 kcal mol^{-1} for increasing order of multibody perturbation theory, and 97.0 and 98.9 kcal mol^{-1} for quadratic configuration interaction without and with triple terms, respectively. Leininger et al.[13] also performed coupled-cluster all-electron and effective core potential calculations, with and without relativistic corrections. They report D_e values of 98.7 (all-electron) and 99.9 kcal mol^{-1} (effective-core potentials) with relativistic corrections, and 100.5 (all-electron) and 100.8 kcal mol^{-1} (effective core) without

TABLE 5: Enthalpy and Internal Energy for Reactions Involving Indium Species[a]

		units in hartree			units in kJ mol^{-1}			units in kcal mol^{-1}		
	reaction	0 K	298.15 K	1000 K	0 K	298.15 K	1000 K	0 K	298.1 K	1000 K
1	$InCl \rightarrow In + Cl$	0.164358	0.165374	0.166558	431.52	434.19	437.30	103.14	103.77	104.52
2	$InCl_3 \rightarrow In+3Cl$	0.360069	0.362481	0.362779	945.36	951.69	952.48	225.95	227.46	227.65
3	$InCl_3 \rightarrow InCl + Cl_2$	0.123190	0.123394	0.121101	323.43	323.97	317.95	77.30	77.43	75.99
4	$InCl_3 \rightarrow InCl + Cl_2$ (no ZPE correction)	0.124269			326.27			77.98		
5	$InF \rightarrow In + F$	0.200840	0.202059	0.203517	527.31	530.51	534.34	126.03	126.79	127.71
6	In_2 triplet $\rightarrow$ 2 In doublet	0.047502	0.048216	0.049291	124.72	126.59	129.41	29.81	30.26	30.93
7	In_2 quintet $\rightarrow$ In doublet + In quartet	0.107672	0.108560	0.109670	282.69	285.03	287.94	67.57	68.12	68.82
8	$In_3 \rightarrow$ 3 In doublet	0.104505	0.105617	0.106637	274.38	277.30	279.98	65.58	66.28	66.92
9	$In_3 \rightarrow$ In doublet + In_2 triplet	0.057003	0.057401	0.057346	149.66	150.71	150.56	35.77	36.02	35.99
10	$InH \rightarrow In + H$	0.099542	0.100950	0.103363	261.35	265.04	271.38	62.46	63.35	64.86
11	$InH_2 \rightarrow InH + H$	0.055206	0.056934	0.058963	144.94	149.48	154.81	34.64	35.73	37.00
12	$InH_2 \rightarrow In + H_2$ (no ZPE correction)	−0.01173			−30.80			−7.36		
13	$InH_3 \rightarrow InH_2 + H$	0.112209	0.114235	0.115649	294.60	299.92	303.64	70.41	71.68	72.57
14	$In(CH_3)H_2 \rightarrow In(CH_3)H + H$	0.109042	0.112107	0.113449	286.29	294.34	297.86	68.43	70.35	71.19
15	$In(CH_3)H \rightarrow In(CH_3) + H$	0.055206	0.056058	0.055815	144.94	147.18	146.54	34.64	35.18	35.02
16	$In(CH_3)_2H \rightarrow In(CH_3)_2 + H$	0.093208	0.096765	0.099561	244.72	254.06	261.40	58.49	60.72	62.48
17	$In_2(CH_3)_4 \rightarrow In(CH_3)_2+In(CH_3)_2$	0.079171	0.075825	0.072448	207.86	199.08	190.21	49.68	47.58	45.46
18	$In(CH_3)_3 \rightarrow In(CH_3)_2 + CH_3$	0.093706	0.093696	0.090609	246.03	246.00	237.89	58.80	58.80	56.86
19	$In(CH_3)_2 \rightarrow In(CH_3) + CH_3$	0.039870	0.039424	0.034900	104.68	103.51	91.63	25.02	24.74	21.90
20	$In(CH_3) \rightarrow In + CH_3$	0.084206	0.085723	0.086092	221.08	225.07	226.03	52.84	53.79	54.02
21	$In(CH_3)_3 \rightarrow In(CH_3)_2(CH_2) + H$	0.156545	0.157773	0.161395	411.01	414.23	423.74	98.23	99.00	101.28
22	$In(CH_3)_2 \rightarrow In(CH_3)(CH_2) + H$	0.156545	0.158931	0.163643	411.01	417.27	429.64	98.23	99.73	102.69
23	$In(CH_3) \rightarrow In(CH_2) + H$	0.153378	0.154526	0.157974	402.69	405.71	414.76	96.25	96.97	99.13
24	$InN \rightarrow In + N$	0.060930	0.062121	0.063526	159.97	163.10	166.79	38.23	38.98	39.86
25	$InN \rightarrow In + {}^1/_2 N_2$	−0.115700	−0.115219	−0.115307	−303.77	−302.51	−302.74	−72.60	−72.30	−72.36
26	In_2N_2 linear $\rightarrow$ 2 InN	0.256513	0.256886	0.254690	673.48	674.45	668.69	160.96	161.20	159.82
27	In_2N_2 linear $\rightarrow$ 2 In + N_2	0.025113	0.026448	0.024075	65.93	69.44	63.21	15.76	16.60	15.11
28	$InP \rightarrow In + P$	0.072204	0.073141	0.074273	189.57	192.03	195.00	45.31	45.90	46.61
29	$InAs \rightarrow In + As$	0.069037	0.069876	0.070969	181.26	183.46	186.33	43.32	43.85	44.53
30	$InSb \rightarrow In + Sb$	0.063337	0.064117	0.065197	166.29	168.34	171.18	39.74	40.23	40.91
31	$(CH_3)_3In:NH_3 \rightarrow In(CH_3)_3 + NH_3$	0.024163	0.025926	0.021310	63.44	68.07	55.95	15.16	16.27	13.37
32	$(CH_3)_3In:N(CH_3)_3 \rightarrow In(CH_3)_3 + N(CH_3)_3$	0.024163	0.021828	0.013384	63.44	57.31	35.14	15.16	13.70	8.40
33	$(CH_3)_3In:NH_3 \rightarrow (CH_3)_2InNH_2 + CH_4$	0.001932	0.003190	0.005546	5.07	8.38	14.56	1.21	2.00	3.48
34	$(CH_3)_2InNH_2 \rightarrow (CH_3)InNH + CH_4$	0.065268	0.065709	0.052485	171.36	172.52	137.80	40.96	41.23	32.93
35	$(CH_3)_3In:N(H_2)N(H_2) \rightarrow In(CH_3)_3 + N_2H_4$	0.023181	0.025124	0.030232	60.86	65.96	79.37	14.55	15.77	18.97
			Internal Energy							
36	$(CH_3)_3In:NH_3 \rightarrow In(CH_3)_3 + NH_3$		0.024976			65.57			15.67	
37	$(CH_3)_3In:N(CH_3)_3 \rightarrow In(CH_3)_3 + N(CH_3)_3$		0.020878			54.82			13.10	

[a] Calculations are based on electronic and vibrational energies obtained using DFT theory.

relativistic corrections. We estimate that the zero-point correction would reduce these values by about 0.4 kcal mol^{-1}. It is interesting to note that, while Bauschlicher's[14] calculations show that the relativistic corrections have a large effect, Leininger et al.[13] calculations indicate differently. Our DFT calculation for the 0K atomization energy of InCl shows excellent agreement with the experimental values, even though no relativistic effects have been considered.

Our calculated bond distance for InCl (Table 3) is 2.471 Å. Huber and Herzberg[19] report a value of 2.401 Å. The calculated values of Schwerdtfeger et al.[15] using multibody perturbation theory, range from 2.411 to 2.412 Å, while using quadratic configuration interaction they obtained 2.413 Å (without triple terms) and 2.414 Å (with triple terms). The all-electron and effective-core potential calculations of Bauschlicher[14] (using quintuple-ζ basis sets) give bond distances of 2.406 and 2.401 Å, respectively. Leininger et al.[13] coupled-cluster calculations range from 2.422 to 2.430 Å. Our value of 2.471 Å is similar to Dobbs and Hehre[17] (2.470 Å) single-determinant Hartree−Fock calculations. Thus, our DFT bond distance is about 3% longer than expected. Coupled cluster and configuration interaction calculations on 10 small molecules using triple-ζ basis sets by Thomas et al.[55]resulted in average errors for bond lengths from −0.69% to +0.20%.

The uncorrected vibrational constant obtained for InCl (Table 4) is 300 cm^{-1}. Huber and Herzberg[19] report 317 cm^{-1}. Bauschlicher's[14] all-electron and effective-core potential calculations give 319 and 317 cm^{-1}, respectively, and the values from Schwerdtfeger et al.[15] range between 308 and 307 cm^{-1} from multibody perturbation theory, and 306 cm^{-1} from quadratic configuration interaction. Leininger et al.[13] report vibrational frequencies of 314−315 cm^{-1} for nonrelativistic calculations, and 306−308 cm^{-1} for relativistic calculations. Our DFT frequency for InCl is 1.05 times smaller than the experimental value or a 5% absolute error. Coupled cluster and configuration interaction calculations on 10 small molecules using triple-ζ basis sets[55]resulted in average absolute percent errors for theoretical harmonic vibrational frequencies ranging between 1.5 ± 2.0% and 6.3 ± 7.4%. Thus, our DFT results for InCl are very satisfactory.

Using the DFT energies of Table 2 the computed atomization energy at 0 K (D_0) for singlet $InCl_3$ (see Table 5, reaction 2) is 225.9 kcal mol^{-1}. On the basis of Barin's[20] experimental standard (298 K) heat of formation for $InCl_3$, Bauschlicher[14] obtains a D_0 of 232.8 kcal mol^{-1}, after performing the corresponding corrections. Bauschlicher's[14] all-electron and effective-core-potential coupled-cluster calculations for $InCl_3$, with no relativistic corrections, result in 256.5 and 242.7 kcal

TABLE 6: Equilibrium Composition for System of Reactions Involving Indium Species[a]

system	ΔG 298.15 K	ΔG 1000 K	equilibrium constant 298.15 K	equilibrium constant 1000 K	molar composition 298.15 K	molar composition 1000 K
System 1: Indium Clusters						
$In_3 \leftrightarrow In_2 + In$		0.027429		1.732×10^{-04}		
$In_2 \leftrightarrow 2\ In$		0.019950		1.837×10^{-03}		
$3\ [In_3] + 2\ [In_2] + [In] = 1$						
$[In]$						0.005
$[In_2]$						0.012
$[In_3]$						0.324
System 2: Indium Hydrides						
$InH_3 \leftrightarrow InH_2 + H$	0.099989	0.064880	1.019×10^{-46}	1.266×10^{-09}		
$InH_2 \leftrightarrow InH + H$	0.047673	0.024005	1.180×10^{-22}	5.105×10^{-04}		
$InH \leftrightarrow In + H$	0.091802	0.068269	5.950×10^{-43}	4.342×10^{-10}		
$H + H \leftrightarrow H_2$	−0.155374	−0.126519	$2.927 \times 10^{+71}$	$2.242 \times 10^{+17}$		
$[InH_3]+[InH_2]+[InH]+[In] = 1$						
$3[InH_3]+2\ [InH_2]+[InH]+[H]+2[H_2] = 2$						
$[H]$					0.000	0.000
$[H_2]$					1.000	1.082
$[In]$					0.000	0.165
$[InH]$					1.000	0.835
$[InH_2]$					0.000	0.000
$[InH_3]$					0.000	0.000
System 3: Trimethylindium Decomposition by In−C Bond Breaking						
$In(CH_3)_3 \leftrightarrow In(CH_3)_2 + CH_3$	0.077526	0.037645	3.636×10^{-36}	6.877×10^{-06}		
$In(CH_3)_2 \leftrightarrow In(CH_3) + CH_3$	0.026576	−0.008120	7.102×10^{-13}	$1.299 \times 10^{+01}$		
$In(CH_3) \leftrightarrow In + CH_3$	0.074274	0.046790	1.115×10^{-34}	3.831×10^{-07}		
$CH_3 + CH_3 \leftrightarrow C_2H_6$	−0.118791	−0.073495	$2.008 \times 10^{+54}$	$1.199 \times 10^{+10}$		
$[In(CH_3)_3]+[In(CH_3)_2]+[In(CH_3)]+[In] = 1$						
$3[In(CH_3)_3]+2\ [In(CH_3)_2]+[In(CH_3)]+[CH_3]+2\ [C_2H_6] = 3$						
$[CH_3]$					0.000	0.000
$[C_2H_6]$					1.000	1.020
$[In]$					0.000	0.040
$[InCH_3]$					1.000	0.960
$[In(CH_3)_2]$					0.000	0.000
$[In(CH_3)_3]$					0.000	0.000
System 4: Trimethylindium Decomposition by In−C and C−H Bond Breaking						
$In(CH_3)_3 \leftrightarrow In(CH_3)_2 + CH_3$		0.037645		6.877×10^{-06}		
$In(CH_3)_2 \leftrightarrow In(CH_3) + CH_3$		−0.008120		$1.299 \times 10^{+01}$		
$In(CH_3) \leftrightarrow In + CH_3$		0.046790		3.831×10^{-07}		
$In(CH_3)_3 \leftrightarrow In(CH_3)_2(CH_2) + H$		0.100364		1.723×10^{-14}		
$In(CH_3)_2 \leftrightarrow In(CH_3)(CH_2) + H$		0.104983		4.007×10^{-15}		
$In(CH_3) \leftrightarrow In(CH_2) + H$		0.106192		2.735×10^{-15}		
$In(CH_3)_2 + In(CH_3)_2 \leftrightarrow In_2(CH_3)_4$		−0.044053		$1.100 \times 10^{+06}$		
$In(CH_3)_2 + H \leftrightarrow In(CH_3)_2H$		−0.041824		$5.441 \times 10^{+05}$		
$In(CH_3) + H \leftrightarrow In(CH_3)H$		−0.019273		$4.396 \times 10^{+02}$		
$In(CH_3)H + H \leftrightarrow In(CH_3)H_2$		−0.067980		$2.102 \times 10^{+09}$		
$In + H \leftrightarrow InH$		−0.067298		$1.695 \times 10^{+09}$		
$InH + H \leftrightarrow InH_2$		−0.024837		$2.547 \times 10^{+03}$		
$InH_2 + H \leftrightarrow InH_3$		−0.063549		$5.188 \times 10^{+08}$		
$In + In \leftrightarrow In_2$		−0.018638		$3.597 \times 10^{+02}$		
$In_2 + In \leftrightarrow In_3$		−0.026607		$4.455 \times 10^{+03}$		
$In(CH_3)_3 + CH_3 \leftrightarrow In(CH_3)_2(CH_2) + CH_4$		−0.014031		$8.398 \times 10^{+01}$		
$In(CH_3)_2(CH_2) \leftrightarrow In(CH_3)(CH_2) + CH_3$		0.042264		1.599×10^{-06}		
$CH_3 + H \leftrightarrow CH_4$		−0.114395		$4.875 \times 10^{+15}$		
$H + H \leftrightarrow H_2$		−0.126521		$2.243 \times 10^{+17}$		
$CH_3 + CH_3 \leftrightarrow C_2H_6$		−0.073495		$1.199 \times 10^{+10}$		
$[In(CH_3)_3]+[In(CH_3)_2]+[In(CH_3)]+[In]+[In(CH_3)_2(CH_2)]+[In(CH_3)(CH_2)]+[In(CH_2)]+2[In_2(CH_3)_4]+$ $[In(CH_3)_2H]+[In(CH_3)H]+[In(CH_3)H_2]+[InH]+[InH_2]+[InH_3]+2[In_2]+3[In_3] = 1$						
$3[In(CH_3)_3]+2[In(CH_3)_2]+[CH_3]+[In(CH_3)]+3[In(CH_3)_2(CH_2)]+2[In(CH_3)(CH_2)]+[In(CH_2)]+$ $4[In_2(CH_3)_4]+2[In(CH_3)_2H]+[In(CH_3)H]+[In(CH_3)H_2]+[CH_4]+2[C_2H_6] = 3$						
$9[In(CH_3)_3]+6[In(CH_3)_2]+3[CH_3]+3[In(CH_3)]+8[In(CH_3)_2(CH_2)]+[H]+5[In(CH_3)(CH_2)]+$ $2[In(CH_2)]+12[In_2(CH_3)_4]+7[In(CH_3)_2H]+4[In(CH_3)H]+5[In(CH_3)H_2]+[InH]+2[InH_2]+3[InH_3]+4[CH_4]+2[H_2]+6[C_2H_6] = 9$						
$[In(CH_3)_3]$						0.000
$[In(CH_3)_2]$						0.000
$[In(CH_3)]$						0.000
$[In(CH_3)_2(CH_2)]$						0.078
$[In(CH_3)(CH_2)]$						0.003
$[In(CH_2)]$						0.000
$[In_2(CH_3)_4]$						0.000
$[In(CH_3)_2H]$						0.000
$[In(CH_3)H]$						0.793
$[In(CH_3)H_2]$						0.000

TABLE 6 (Continued)

system	ΔG 298.15 K	ΔG 1000 K	equilibrium constant 298.15 K	equilibrium constant 1000 K	molar composition 298.15 K	molar composition 1000 K
[In]						0.000
[In_2]						0.000
[In_3]						0.000
[InH]						0.000
[InH_2]						0.000
[InH_3]						0.000
[H]						0.003
[H_2]						0.043
[CH_3]						0.000
[CH_4]						0.000
[C_2H_6]						1.199
System 5: Trimethylindium Decomposition plus Amine Adduct Formation						
$In(CH_3)_3 \leftrightarrow In(CH_3)_2 + CH_3$	0.077526	0.037645	3.636×10^{-36}	6.877×10^{-06}		
$In(CH_3)_2 \leftrightarrow In(CH_3) + CH_3$	0.026576	−0.008120	7.102×10^{-13}	$1.299 \times 10^{+01}$		
$In(CH_3) \leftrightarrow In + CH_3$	0.074274	0.046790	1.115×10^{-34}	3.831×10^{-07}		
$CH_3 + CH_3 \leftrightarrow C_2H_6$	−0.118791	−0.073495	$2.008 \times 10^{+54}$	$1.199 \times 10^{+10}$		
$In(CH_3)_3+NH_3 \leftrightarrow (CH_3)_3In:NH_3$	−0.011733	0.021027	$2.309 \times 10^{+05}$	1.307×10^{-03}		
$[In(CH_3)_3]+[In(CH_3)_2]+[In(CH_3)]+[In]+[(CH_3)_3In:NH_3] = 1$						
$3[In(CH_3)_3]+2[In(CH_3)_2]+[In(CH_3)]+[CH_3]+2[C_2H_6]+3[CH_3)_3InNH_3] = 3$						
$[NH_3]+[(CH_3)_3In:NH_3] = 1$						
[CH_3]					0.000	0.000
[C_2H_6]					0.961	1.020
[In]					0.000	0.040
[$InCH_3$]					0.961	0.960
[$In(CH_3)_2$]					0.000	0.000
[$In(CH_3)_3$]					0.000	0.000
[NH_3]					0.961	1.000
[$(CH_3)_3InNH_3$]					0.039	0.000
System 6: Trimethylindium Decomposition plus Trimethylamine Adduct Formation						
$In(CH_3)_3 \leftrightarrow In(CH_3)_2 + CH_3$	0.077526	0.037645	3.636×10^{-36}	6.877×10^{-06}		
$In(CH_3)_2 \leftrightarrow In(CH_3) + CH_3$	0.026576	−0.008120	7.102×10^{-13}	$1.299 \times 10^{+01}$		
$In(CH_3) \leftrightarrow In + CH_3$	0.074274	0.046790	1.115×10^{-34}	3.831×10^{-07}		
$CH_3 + CH_3 \leftrightarrow C_2H_6$	−0.118791	−0.073495	$2.008 \times 10^{+54}$	$1.199 \times 10^{+10}$		
$In(CH_3)_3+N(CH_3)_3 \leftrightarrow (CH_3)_3In:N(CH_3)_3$	−0.006353	0.039526	$8.019 \times 10^{+02}$	3.797×10^{-06}		
$[In(CH_3)_3]+[In(CH_3)_2]+[In(CH_3)]+[In]+[(CH_3)_3In:N(CH_3)_3] = 1$						
$3[In(CH_3)_3]+2\ [In(CH_3)_2]+[In(CH_3)]+[CH_3]+2[C_2H_6]+3[(CH_3)_3In:N(CH_3)_3] = 3$						
$[N(CH_3)_3]+[(CH_3)_3In:N(CH_3)_3] = 1$						
[CH_3]					0.000	0.000
[C_2H_6]					1.000	1.020
[In]					0.000	0.040
[$InCH_3$]					1.000	0.960
[$In(CH_3)_2$]					0.000	0.000
[$In(CH_3)_3$]					0.000	0.000
[$N(CH_3)_3$]					1.000	1.000
[$(CH_3)_3In:N(CH_3)_3$]					0.000	0.000
System 7: Dimerization of Indium Nitride						
$InN + InN \leftrightarrow In_2N_2$		−0.200919		$3.579 \times 10^{+27}$		
$In_2N_2 \leftrightarrow 2\ In + N_2$		−0.049026		$5.289 \times 10^{+06}$		
$2\ In \leftrightarrow In_2$		−0.019950		$5.444 \times 10^{+02}$		
$In_2 + In \leftrightarrow In_3$		−0.027429		$5.774 \times 10^{+03}$		
$[InN]+2[In_2N_2]+[In]+2[In_2]+3[In_3] = 1$						
$[InN]+2[In_2N_2]+2[N_2] = 1$						
[InN]						0.000
[In_2N_2]						0.000
[In]						0.005
[In_2]						0.012
[In_3]						0.324
[N_2]						0.500

[a] Calculations are based on electronic and vibrational energies obtained using DFT theory. Units of Gibbs free energy: hartree.

mol^{-1}, respectively, and 232.7 and 234.1 kcal mol^{-1}, after relativistic corrections. The coupled-cluster calculations by Schwerdtfeger et al.[15] with relativistic pseudopotentials, result in decomposition energies at 0 K ($InCl_3 \rightarrow InCl + Cl_2$) with no zero-point corrections ranging from 369.1 to 341.1 kJ mol^{-1} for increasing order of multibody perturbation theory, and 339.3 and 338.0 kJ mol^{-1} for quadratic configuration interaction without and with triple terms, respectively. These values are compared with a decomposition value of 302.5 kJ mol^{-1} derived from Barin's[20] standard heat of formation data. Our decomposition energy, with no zero-point correction, for $InCl_3$ is 326.3 kJ mol^{-1} (Table 5, reaction 4). Our calculated atomization energy is 7.5 kcal mol^{-1} lower than Bauschlicher's[14] estimated experimental value and our calculated decomposition energy is 23.8 kJ mol^{-1} (5.7 kcal mol^{-1}) higher than Schwerdtfeger et al.[15] estimated experimental value. Thus, our DFT energy calculation for $InCl_3$ is in reasonable agreement with experimental results.

TABLE 7: Molecular Properties for InCl and $InCl_3$[a]

	InCl			$InCl_3$						
	D_0 (kcal mol^{-1})	R_e (Å)	ν (cm^{-1})	D_0 (kcal mol^{-1})	ΔE (kJ mol^{-1})	R_e In−Cl (Å)	ν (cm^{-1}) E′	A_1′	A_2″	E′
DFT calculation	103.1	2.471	300	225.9	326.3	2.347	381	332	90	84
experimental values										
ref 16	102.4	2.401	317							
ref 17/ref 11	103.5			232.8						
ref 17/ref 12					302.5					
ref 19						2.275	379	344	110	100
other calculations										
ref 11: CCSD(T); AE; CBS	109.1	2.406[b]	319[b]	256.5						
ref 11: CCSD(T); ECP; CBS	108.6	2.401[b]	317[b]	242.7						
ref 11: CCSD(T); AE; CBS; RC	102.8			232.7						
ref 11: CCSD(T); ECP; CBS; RC	103.5			234.1						
ref 12: MP2-MP4; ECP + RC	102.8−97.3	2.411−2.412	308−307		369.1−341.1	2.292	396[c]	348	110	100
ref 12: QCISD-QCISD(T); ECP + RC	97.0−98.9	2.413−2.414	306		339.3−338.0	2.295−2.299				
ref 10: CCSD; AE	100.5[d]	2.426	314							
ref 10: CCSD; ECP	100.8[d]	2.422	315							
ref 10: CCSD; AE; RC	98.7[d]	2.430	306							
ref 10: CCSD; ECP; RC	99.9[d]	2.426	308							
ref 14: HF		2.470								
ref 15: MP2						2.248	382	344	120	115

[a] Code: AE = all electron; CBS = complete basis set extrapolation; CCSD(T) = coupled cluster including single, double, and optional triple terms; D_0 = 0 K atomization energy; ECP = effective-core potential; MP2-MP4 = multibody perturbation theory, orders 2−4; QCISD = quadratic configuration interaction including single and double terms; QCISD(T) = quadratic configuration interaction including triple terms; RC = relativistic corrections; R_e = equilibrium bond distance; ν = vibrational frequency; ΔE = 0 K decomposition energy ($InCl_3 \rightarrow InCl + Cl_2$) with no zero-point energy correction. [b] Using quintuple-ζ basis sets. [c] MP3 result. [d] D_e values. We estimate that the zero-point energy for InCl would reduce these values by about 0.4 kcal mol^{-1}.

Our calculated In−Cl distance in $InCl_3$ (Table 3) is 2.347 Å. From a combined analysis of gas electron diffraction intensities and vibrational frequencies, the experimental distance was determined to be 2.275 Å.[22] The calculation of Schwerdtfeger et al.[15] using multibody perturbation theory results in 2.292 Å, while the quadratic configuration interaction calculation gives 2.295 Å (without triple terms) and 2.299 Å (with triple terms). Okamoto's[18] multibody perturbation calculation gives a bond distance of 2.248 Å. Our DFT In−Cl bond distance in $InCl_3$ is about 3% longer than the experimental distance, similarly to InCl.

The uncorrected vibrational constants obtained for $InCl_3$ (see Table 4) are 381 (E′), 332 (A_1′), 90 (A_2″), and 84 (E′) cm^{-1}. The experimental values of Vogt et al.[22] are 379 (E′), 344 (A_1′), 110 (A_2″), and 100 (E′) cm^{-1}. The results from Schwerdtfeger et al.[15] using third-order multibody perturbation theory are 396 (E′), 348 (A_1′), 110 (A_2″), and 100 (E′) cm^{-1}. Finally, Leininger et al.[13] give the following values: 382 (E′), 344 (A_1′), 120 (A_2″), and 115 (E′) cm^{-1}. Our DFT frequencies for $InCl_3$ have to be multiplied by the following factors to obtain the experimental values: 0.99, 1.04, 1.22, and 1.19, thus ranging the absolute error from 0.5% for the larger vibration to 16% for the smallest. For comparison, the values of Schwerdtfeger et al.[15] should be multiplied by 0.96, 0.99, 1.00, and 1.00, thus having absolute errors between 4.5% and 0%.

Figure 3 shows the molecular orbital diagram obtained for InCl and $InCl_3$, respectively. Both InCl and $InCl_3$ display a drop in energy of the In 5s electrons. The Cl 3s orbital increases in energy in InCl but these atomic orbitals are almost unaffected in $InCl_3$ (similarly to the Cl 3p lone-pair electrons, which have a small increase in energy in InCl and are almost unaffected in $InCl_3$). In InCl, bonding occurs between a high energy In 5p and lower energy Cl $3p_z$ (displayed in Figure 3 with a dashed line). The three bonding orbitals in $InCl_3$ are considerably lower in energy than the bonding orbital in InCl, even lower than the 3p lone pairs in Cl. Finally, the 4d In atomic orbitals are considerably perturbed in $InCl_3$. This effect is consistent with the larger effective charge on the In atom in $InCl_3$ (+1.02) than in InCl (+0.49), producing a contraction of the 4d orbitals.

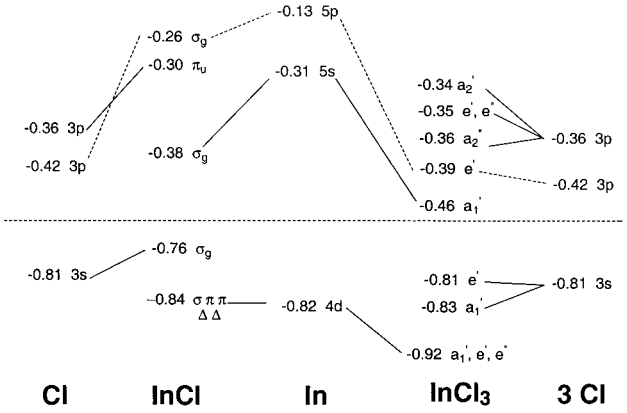

Figure 3. Molecular orbital diagram for indium chloride and indium trichloride (energy units: hartree).

Our DFT calculations on InF result in a D_e value of 126.4 kcal mol^{-1} or a D_0 value of 125.6 kcal mol^{-1}. Leininger et al.[13] report D_e values of 125.7 and 125.4 kcal mol^{-1}, based on two coupled-cluster calculations with 20 and 28 correlated electrons, respectively, and including relativistic effects. The D_e experi-

mental value[19] is 126.4 cm^{-1}. Our DFT calculation for InF is the same as the experimental value, and about 0.7 kcal mol^{-1} above the coupled-cluster calculations with relativistic effects.

The DFT equilibrium distance obtained for InF was 2.020 Å (see Table 3). The experimental value[19] was reported as 1.985 Å. The coupled-cluster relativistic calculations of Leininger et al.[13] gave a value of 1.990 Å and the Hartree−Fock calculations of Dobbs and Hehre[17] resulted in 1.943 Å. In the case of InF, our bond distance is overestimated by about 2%, while the coupled-cluster calculation overestimates by only 0.3%. On the other hand, the Hartree−Fock calculation underestimates by 2%.

Table 4 shows an estimated vibrational frequency of 551 cm^{-1} for InF. The experimental value[19] is 535.3 cm^{-1}, while Leininger et al.[13] report 526 cm^{-1}. Our value overestimates the property by a factor of 1.03.

Indium Clusters. Atomic indium has been observed by resonant fluorescence spectroscopy produced by the pyrolysis of $In(CH_3)_3$ at temperatures above 600 K.[56] Furthermore, the pyrolysis of $In(CH_3)_3$ at temperatures above 400 °C was seen to occur mostly homogeneously in the gas phase.[34] Thus, OMCVD reactors may contain In clusters.

We considered the singlet, triplet and quintet states of In_2, and the linear, bent and triangular conformations of doublet and quartet In_3. No stable In_2 singlet state was achieved. The two stable states of In_2 found are $^3\pi_u$ and $^5\Sigma_u$ (see Table 2), with bond distances of 2.811 and 2.658 Å, respectively (Table 3). The two stable states found for the In_3 molecule correspond to a bent $^4A_2$ and a linear $^4\Sigma_u$ state (Table 2), with bond distances of 2.948 and 2.875 Å (Table 3), respectively.

Multiconfiguration self-consistent-field calculations with relativistic corrections by Balasubramanian and Li,[30] and energy-adjusted pseudopotential calculations by Ingel-Mann et al.[32] also found the $^3\pi_u$ state to be the ground state of In_2. Balasubramanian and Li[30] report a bond distance of 3.0 Å, vibrational frequency of 135 cm^{-1} and D_e of 80 kJ mol^{-1}, and Ingel-Mann et al.[32] report a D_e of 105 kJ mol^{-1}. From all-gas equilibria spectrometric measurements, a D_0 for In_2 of 74.4 ± 5.7 kJ mol^{-1} was recently obtained by Balducci et al.[29] The heat of atomization at 0 K, corresponding to eqs 6 from Table 5, was calculated to be 125 kJ mol^{-1}, 1.7 times higher than the calculated D_0 of Balducci et al.[29] and 1.2 times higher than that calculated by Ingel-Mann et al.[32] Earlier experimental values based on mass spectrometry have been reported by De Maria et al.[57] (93.7 kJ mol^{-1}, for a Σ state), Drowart and Honig[58] (96.5 kJ mol^{-1}) and Gingerich and Blue[59] (102.5 kJ mol^{-1}). Huber and Herzberg[19] report 97 kJ mol^{-1}, a value that was corrected by Froben et al.[60] to 84 kJ mol^{-1} after a 118 cm^{-1} frequency was measured in Raman spectra of matrix-isolated group IIIA dimers. We obtained a vibrational frequency of 107 cm^{-1} (Table 4), a factor of 1.10 smaller than the one determined by Froben et al.[60] In_2 ground state is a weakly bound free-radical molecule that may contain 75 vibrational quantum levels, assuming a harmonic oscillator approximation.

Our DFT calculations resulted in two stable quartet In_3 states, corresponding to a bent ($^4A_2$) and a linear ($^4\Sigma_u^-$) structure. The bent state is lower in energy by only 8 kJ mol^{-1}, has a bond distance of 2.948 Å, an angle of 76°, vibrational frequencies of 41(A_1), 121(B_2), and 127(A_1) cm^{-1}, and an atomization energy of 269 kJ mol^{-1} (Tables 5, reaction 8). The linear state has a bond distance of 2.875 Å and vibrational frequencies of 45(π_u), 97(σ_g) and 165(σ_u) cm^{-1}. Complete-active space multiconfiguration self-consistent-field calculations performed by Feng and Balasubramanian,[31] followed by multireference singles and doubles configuration interaction with relativistic corrections, resulted in an isosceles structure ($^4A_2$), with a 0K dissociation energy of 201 kJ mol^{-1}, considerably weaker than the one predicted by our calculations. The corresponding linear structure ($^4\Sigma_u^-$) was found to be only 7 kJ mol^{-1} of higher energy. The bond distances they report are two of 2.95 Å and an angle of 71° for the $^4A_2$ state, and 2.90 Å for the $^4\Sigma_u^-$ state.

The standard Gibbs free energy for the dissociation of In_3 (eq 9 of Table 5) using data from Table 8, Appendix 1, was calculated to be 127 kJ mol^{-1}, indicating that In_3 is also a weakly bound free-radical species. The standard Gibbs free energy for the dissociation of In_2 was calculated to be 105 kJ mol^{-1}. Temperature-dependent calculations of Gibbs free energy for the dissociation of ground-state In_2 and In_3 give spontaneous dissociation above 1370 and 2170K, respectively.

Equilibrium composition for the three species (In, In_2, and In_3), were estimated for 1000K using a mass balance equation on the In atom (Table 6, system 1). The resulting proportions for In, In_2, and In_3, respectively, are 10^{-2}:10^{-2}:1 at 1000 K. The equilibrium constants for the In_2 and In_3 dissociations are 10^{-3} and 10^{-4}, respectively. Consequently, for 1 atm gaseous indium and at 1000 K one expects about 0.5% to be as In atom and 2.4% as In dimer (In_2).

Indium Hydrides. The hydrides considered were InH singlet and triplet, InH_2 doublet, and InH_3 singlet. The diatomic singlet was found to be lower in energy than the triplet state. The In−H distance becomes smaller with increasing number of H's (see Table 3): 1.878 Å in InH, 1.799 Å in InH_2, and 1.766 Å in InH_3. The H−In−H angle in InH_2 is 119°. The 0 K atomization energies D_0 for InH, InH_2, and InH_3 were calculated to be (on the basis of reactions 10, 11, and 13 of Table 5): 261, 406, and 701 kJ mol^{-1}, respectively, or D_e of 270, 429, and 743 kJ mol^{-1}, respectively. The frequencies obtained are 1442 cm^{-1} for InH; 612, 1615, and 1666 cm^{-1} for InH_2; and 602(A_2"), 608(E′), 1761(E′), and 1766(A_1′) for InH_3.

The singlet state of InH was calculated to have a 1.86 Å bond distance, a frequency of 1482 cm^{-1}, and a D_e of 240 kJ mol^{-1} by Teichteil and Spiegelmann,[23] using relativistic configuration interaction methods. Using complete active space SCF followed by full second-order configuration interaction and relativistic calculations Balasumbramanian[24] obtained a bond distance of 1.823 Å for the singlet, a D_e of 249 kJ mol^{-1} and a vibrational frequency of 1469 cm^{-1}. DFT calculations by Pullumbi et al.[11] give a vibrational frequency of 1466 cm^{-1} and a bond distance of 1.89 Å, while coupled-cluster calculations performed by the same authors with single, double and triple excitations, give a vibrational frequency of 1504 cm^{-1} and a bond distance of 1.850 Å. In addition, coupled-cluster calculations with single and double excitations (using pseudopotentials and scalar-relativistic energy corrections) resulted in a dissociation energy of 255 kJ mol^{-1}, a bond length of 1.846 Å, and a vibrational frequency[13] of 1432 cm^{-1}. From an experimental point of view, Huber and Herzberg[19] report a D_e of 248 kJ mol^{-1}, a bond distance of 1.8378 Å, and a vibrational frequency of 1475.4 cm^{-1}; and Rosen[28] reports the same D_e, a bond distance of 1.89 Å, and a vibrational frequency of 1476 cm^{-1}. From IR studies, Bahnmaier et al.[26] report a bond distance of 1.83776 Å, a vibrational frequency of 1475 cm^{-1}, and White et al.[27] report a D_e of 248 kJ mol^{-1}, a bond distance of 1.836 Å, and a vibrational frequency of 1476 cm^{-1}.

Our bond distance for singlet InH lies within the reported experimental values. Our D_e (270 kJ mol^{-1}) is 9% higher than the experimental; and our vibrational frequency is 1.02 times smaller than the experimental values.

Our InH triplet state was found to be 193 kJ mol^{-1} higher in

energy than the singlet, to have a bond distance of 1.813 Å and a vibrational frequency of 1483 cm^{-1}. Teichteil and Spiegelmann[23] found the triplet state to be 176 kJ mol^{-1} higher in energy than the singlet, to have a bond distance of 1.79 Å and a vibrational frequency of 1511 cm^{-1}. Balasumbramanian[24] found it to be 177 kJ mol^{-1} higher in energy, to have a bond distance of 1.749 Å and a vibrational frequency of 1503 cm^{-1}. Rosen[28] reports an experimental value 195 kJ mol^{-1} higher for the triplet than for the singlet state, having the triplet a bond distance of 1.78 Å and a vibrational frequency of 1459 cm^{-1}. Similarly, Huber and Herzberg[19] report an energy difference of 194 kJ mol^{-1} between the triplet and the singlet states, a bond distance of 1.776 Å and a vibrational frequency of 1304 cm^{-1}, for the triplet state. The difference in energy between the singlet and the triplet states that we obtained is very similar to the experimental values; the bond distance is about 2% the experimental values; and, the vibrational frequency is about 2% higher than Rosen's[28] value.

We obtained a stable calculation of a bent conformation for doublet InH_2. The In−H bond distance were 1.799 Å, the H−In−H angle was 199°, and the vibrational frequencies were 1666, 1615, and 612 cm^{-1}. The 0 K dissociation energy D_0 into InH + H was calculated to be 145 kJ mol^{-1} and into In + H_2 (with no zero-point energy correction) −31 kJ mol^{-1} (see Table 5, reactions 11 and 12). Pullumbi et al.[11] have synthesized InH_2 by reacting molecular hydrogen and excited metal atoms isolated in solid argon and have performed DFT and coupled-cluster calculations with single and double excitations on this molecule. Their IR measurements in solid argon resulted in vibrational frequencies of 1615.6, 1548.6, and 607.4 cm^{-1}, while their DFT calculations resulted in frequencies of 1608.8, 1561.8, and 621.6 cm^{-1}; a In−H bond distance of 1.815 Å; and a H−In−H angle of 120.58°. Multiconfiguration self-consistent field calculations with second-order configuration interaction with relativistic effects performed by Balasubramanian and Tao,[25] resulted in 0 K dissociation energy (with no zero-point energy corrections) of −50 kJ mol^{-1} with respect to In + H_2 and 132 kJ mol^{-1} with respect to InH + H. They also obtained a bond distance of 1.782 Å, and a bond angle of 119.7°. Our calculated dissociation energy for the splitting of one H atom is 15 kJ mol^{-1} higher than the calculations of Balasubramanian and Tao;[25] our bond distance is between their value and the value by Pullumbi et al.,[11] and our vibrational frequencies are less than 1.04 times larger than the IR measurements.

We found the D_{3h} conformation of InH_3 to be the ground state, with an In−H bond distance of 1.766 Å, vibrational frequencies of 602(A_2''), 608(E′), 1761(E′), and 1766(A_1'), and a 0K D_0 of 295 kJ mol^{-1}. (Table 5, Reaction 13), or D_e of 314 kJ mol^{-1}. The already mentioned calculations by Balasubramanian and Tao[25] give a bond distance of 1.754 Å and a D_e of 292 kJ mol^{-1}. Dobbs and Hehre report a calculated bond distance of 1.781 Å. Vibrational frequencies from IR measurements in solid argon[12] found In−H stretching frequencies at around 1754.5 cm^{-1}; and bending frequencies of 613.2 and 607.8 cm^{-1}. Consequently, our D_e is 7% higher than the value calculated by Balasubramanian and Tao;[25] our bond distance is less than 1% larger than their value; and, our vibrational frequencies are less than 1% different from the experimental values.

System 2 of Table 6 was utilized to calculate the equilibrium composition of ground-state gaseous indium hydrides at 298.15 and 1000K (based on Table 8, Appendix 1, data) in molecular H_2. A 1:1 ratio of indium atoms and molecular H_2 is represented by the last two mass balance equations. The equilibrium constants obtained at 298.15 K for dissociation of a H atom from InH_3, InH_2, and InH were 10^{-46}, 10^{-22}, and 10^{-42}, respectively, and at 1000 K were 10^{-9}, 10^{-4}, and 10^{-10}, respectively. For a system at equilibrium that initially contained In atoms and H_2 molecules in a ratio of 1:1, only InH would be present at 298.15 K, but at 1000 K, the percent of InH would drop to 84%, with 17% of the indium as In atoms.

Indium Alkylides, and Their Hydrogen and Dehydrogenated Derivatives. The species considered in this group include hydrogen and dehydrogenated derivatives of the indium alkylides. The 10 species are methylindium [$In(CH_3)$] and its derivatives [$In(CH_3)H$, $In(CH_3)H_2$, $In(CH_2)$], dimethylindium [$In(CH_3)_2$] and its derivatives [$In(CH_3)_2H$, $In(CH_3)CH_2$, $In_2(CH_3)_4$)], and trimethylindium [$In(CH_3)_3$] and its dehydrogenated derivative $In(CH_3)_2CH_2$.

In the case of methylindium [$In(CH_3)$], a singlet C_{3v} state and a triplet C_s state were found to be stable, with the singlet being 188 kJ mol^{-1} lower in energy than the triplet. The 0 K dissociation energy into In and CH_3 was calculated to be 221 kJ mol^{-1} (Table 5, reaction 20). Its corresponding hydrogenated derivatives [$In(CH_3)H_2$ and $In(CH_3)H$] had 0 K dissociation energies (for loosing one H atom) of 286 and 145 kJ mol^{-1}, respectively (Table 5, reactions 14 and 15). Figure 4 depicts the structure of the $In(CH_3)H$ radical, where one of the methyl H's is cis and coplanar to the singly occupied In orbital and trans to the H atom bonded to In. Figure 4 also shows the structure of the $In(CH_3)H_2$ molecule, where the two H atoms attached to In are coplanar to one of the methyl H atoms. Multibody perturbation calculations by El-Nahas and Schleyer[33] on $In(CH_3)H_2$ show an In−C bond distance of 2.205 Å, less than half a percent larger than our value (see Table 3), and a zero-point energy correction of 0.04725 hartree, 2% higher than our value (see Table 2). We found that the dehydrogenated species of methylindium, the doublet $In(CH_2)$, has an In−C bond distance about 1% smaller than methylindium. The 0 K dissociation energy for methylindium into this species plus a hydrogen atom was calculated to be 403 kJ mol^{-1} (Table 5, reaction 23).

The doublet dimethylindium $In(CH_3)_2$ may form a singlet dimer, stable by about 208 kJ mol^{-1} (Table 5, reaction 17) with respect to two monomers. Figure 4 sketches the dimethylindium dimer, with an In−In distance of 2.847 Å and D_2 symmetry. On the other hand, the dimethylindium dissociation energy (Table 5, reaction 19) into methylindium and methyl radical was calculated to be only 105 kJ mol^{-1}. Two stable singlet structures were found for the hydrogenated dimethylindium molecule [$In(CH_3)_2H$], of conformations quasi C_s and quasi C_{2v}. The former was found to be only 46 kJ mol^{-1} lower in energy. Dissociation of the H atom (at 0 K) requires 245 kJ mol^{-1} (Table 5, Reaction 16). Finally, the formation of the dehydrogenated species $In(CH_3)CH_2$ from dimethylindium requires 411 kJ mol^{-1} of energy (Table 5, Reaction 22). The In−C bond distances in these species were found to be 2.242 Å for dimethylindium, 2.200 Å for the hydrogenated species, 2.165 Å for the dehydrogenated species, and 2.218 Å for the dimethylindium dimer.

Trimethylindium [$In(CH_3)_3$] is a conventional organometallic precursor of OMCVD for groups III and V semiconductors. Dissociation into dimethylindium plus a methyl radical at 0 K was calculated to be 246 kJ mol^{-1} (Table 5, reaction 18), whereas the dehydrogenation of trimethylindium into $In(CH_3)_2CH_2$ was estimated to be 411 kJ mol^{-1} (Table 5, reaction 21). The C_{3v} structure of trimethylindium is shown in Figure 4, with all heavy atoms on the same plane. The calculated In−C bond

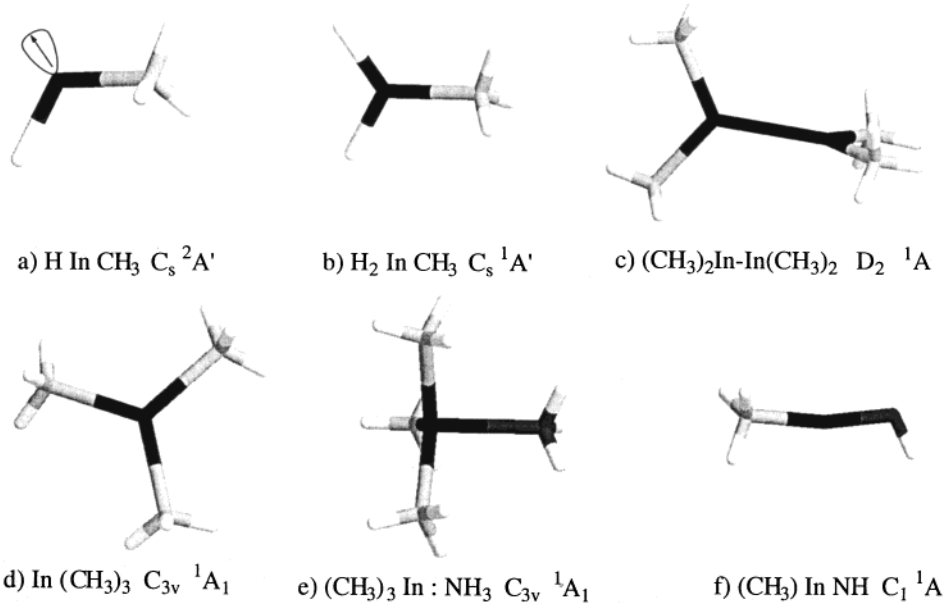

Figure 4. Diagrams of indium compounds. The four grades correspond, from dark to light, to indium, nitrogen, carbon, and hydrogen atoms.

distances for trimethylindium are 2.208 Å, and the dehydrated radical has two bonds of 2.203 Å and one of 2.171 Å.

One of the most important issues in OMCVD is the process of metallic precursor decomposition. A study by Larsen et al.[61] on the thermal decomposition of trimethylgallium [$Ga(CH_3)_3$] showed that attack of this molecule by a methyl radical probably results in methane and $Ga(CH_3)_2CH_2$, which would then decompose to $Ga(CH_3)(CH_2)$. Similar reactions for trimethylindium are

$$In(CH_3)_3 + CH_3 \rightarrow CH_4 + In(CH_3)_2(CH_2) \qquad (10)$$

$$In(CH_3)_2(CH_2) \rightarrow CH_3 + In(CH_3)(CH_2) \qquad (11)$$

Using the data of Table 8, Appendix 1, calculation of the Gibbs free energy for eq 10 gives -19 kJ mol^{-1} at 300 K and -7kJ mol^{-1} at 1000 K, thus resulting in a spontaneous reaction except at very high temperatures. For eq 11, similar calculations give 213 kJ mol^{-1} at 300 K and 148 kJ mol^{-1} at 1000 K, an unfavorable reaction that improves with increasing temperature.

The decomposition of trimethylindium into methylindium and two methyl radicals is believed to be the initiating steps of a chain reaction in D_2 or toluene (an efficient radical scavenger), with the formation of ethane:[34]

$$In(CH_3)_3 \rightarrow In(CH_3)_2 + CH_3 \rightarrow In(CH_3) + 2CH_3 \qquad (12)$$

$$CH_3 + CH_3 + M \rightarrow C_2H_6 + M \qquad (13)$$

In 1963, Jacko and Price[62] proposed that trimethylindium decomposes by homolytic fission loosing two methyl radicals in rapid succession to form methylindium, where the rate constant for breaking the second methyl bond is much higher than that for the first bond. Larsen et al.[61] proposed that a chain reaction occurs during pyrolysis, triggered by the formation of methyl radicals.

Buchan et al.[63] determined that trimethylindium pyrolyzes mostly homogeneously in the gas phase when it is alone, but in the presence of phosphine (PH_3) both components pyrolyze at lower temperatures than alone and only methane (CH_4) is formed. In this case, InP is initiated by the reaction of trimethylindium and phosphine in the vapor phase. An activation energy of 150 kJ mol^{-1} was found for the homogeneous decomposition in H_2, but the decomposition was found to be surface dependent when N_2 was used as a carrier gas.[64] The reaction was believed to be heterogeneous at temperatures below 673K and homogeneous at higher temperatures. In the case of an heterogeneous reaction (lower temperatures) the possibility of adduct formation between trimethylindium and phosphine was proposed.

The methyl dissociation of trimethylindium adsorbed at a GaAs substrate was studied at 300 K by Shogen et al.[65] and that adsorbed at a Si(11) substrate was studied at various temperatures by Bu et al.[66] The latter investigation determined that there is partial In−C dissociation at 120 K; at 550 C−H breaking occurs; at 630 K, In form islands and desorbs; and at temperatures above 950 K, there is complete H and In desorption and only Si−C is left. Measurements of atomic In during pyrolysis of trimethylindium were obtained by Hebner et al.[67] using resonant fluorescence spectroscopy, with a threshold temperature for observation of indium signal of 598 K. The decomposition of trimethylindium using H_2 as a carrier gas was also studied by Fan et al.[68] The kinetics of trimethylindium pyrolysis was studied using mass spectrometry sampling by Allendork et al.[69] They determined an activation energy of 193 kJ mol^{-1}.

Two equilibrium systems were considered for the dissociation of trimethylindium: one with only In−C bond breaking (Table 6, system 3) and one with both In−C and C−H bond breaking (Table 6, system 4). In the first case the radicals formed are dimethylindium, methylindium, indium atom and methyl, at 298.15 and 1000 K. In the second case, all of the alkylindium derivatives (hydrogenated and dehydrated) are included, plus the indium hydrides and indium clusters, at 1000 K. In system 3 the methyl radicals combine to form ethane, while in system 4 the H atoms and the methyl radicals combine to form H_2, CH_4, and C_2H_6. In system 3 and at room temperature the dominant species present are $In(CH_3)$ and C_2H_6, but at 1000 K 10% of free In atoms are also present (notice that this system does not consider cluster formation). In system 4, and at 1000 K, the hydrocarbon present is C_2H_6, (no CH_4 nor H_2); most of the indium is as In_3 (38%), about 37% as $In(CH_2)$, 2% as In_2, and less than 1% as $In(CH_3)$ and In atoms. It should be noted

that for the system with 21 equations the mass balance equation was achieved within 10%.

Trimethylindium Adducts with Ammonia, Trimethylamine, Hydrazine, and Derivatives. Trimethylindium with ammonia, trimethylamine and hydrazine are common precursors in OMCVD experiments.[4] Adducts may form between groups III and V compounds, which may dissociate or decompose by eliminating alkanes. For example, trimethylindium adducts with trimethylphospine or triethylphospine were seen to dissociate[70] but trimethylindium with arsine[71] to decompose. Larsen et al.[72] and Buchan et al.[34] proposed formation of an adduct between trimethylindium and phosphine as a possible low-temperature mechanism during the pyrolysis of trimethylindium and phosphine, with decomposition into $(CH_3)_2InPH_2$ plus methane. In particular, we studied the trimethylindium adduct with ammonia $[(CH_3)_3In{:}NH_3]$, the trimethylindium adduct with trimethylamine, $[(CH_3)_3In{:}N(CH_3)_3]$, the trimethylindium adduct with hydrazine $[(CH_3)_3In{:}N(H_2)N(H_2)]$, and the derivatives $(CH_3)_2InNH_2$, singlet and triplet $(CH_3)InNH$.

$(CH_3)_3In{:}NH_3$ was found to have C_{3v} symmetry, with the trimethylindium almost retaining its heavy atoms coplanar. Figure 4 shows the small puckering of the trimethylindium part resulting from the In−N bonding. The In−N distance was found to be 2.450 Å (Table 3), while the In−C bonds became 0.7% larger than in trimethylindium. Dissociation enthalpy for this adduct was calculated to be 64 kJ mol^{-1} at room temperature (Table 5, Reaction 31). The trimethylindium adduct with trimethylamine $[(CH_3)_3In{:}N(CH_3)_3]$ was also found to be C_{3v}, with a 1% larger In−N bond distance (2.476 Å) and similar In−C bond lengths than the ammonia adduct. The dissociation enthalpy for the trimethylamine adduct (Table 5, reaction 32) was calculated to be 62 kJ mol^{-1} at room temperature, and a change in internal energy (Table 5, Reaction 37) of 60 kJ mol^{-1}. The trimethylindium adduct with hydrazine $[(CH_3)_3In{:}N(H_2)N(H_2)]$ has an In−N bond distance of 2.453 Å, barely larger than the adduct with ammonia, and has a dissociation enthalpy of 62 kJ mol^{-1} at room temperature (Table 5, reaction 35). The derivative obtained after eliminating a methane molecule from the amine adduct [See Figure 4, $(CH_3)_2InNH_2$] shows an In−N distance 16% smaller. The enthalpy for the methane elimination was found to be only 13 kJ mol^{-1} at room temperature. Subsequent elimination of a methane would require 171 kJ mol^{-1} (Table 5, reaction 34).

Bradley et al.[35] determined the structure of the trimethylamine adduct of trimethylindium by electron diffraction, and the enthalpy and the internal energy change for the dissociation by electron diffraction and infrared spectroscopy. They found a C_{3v} structure, with $In(CH_3)_3$ almost retaining its planar structure. Their In−N bond distance of 2.378 Å is 4% smaller than our calculation, whereas their In−C distance of 2.170 Å is less than 3% smaller than our calculation. From the relative amounts of the three species in the vapor at 335, 374, 426, and 474 K obtained by electron diffraction, an enthalpy of dissociation of 81 ± 6 kJ mol^{-1} was obtained, 23% larger than our value. For the dissociation at constant volume, and using infrared spectroscopy to determine relative concentrations at six temperatures between 298 and 427 K, the value of 84 ± 2 kJ mol^{-1} was obtained, 26% higher than our calculated 62 kJ mol^{-1}.

The adduct formation was incorporated into the small system for the trimethylindium decomposition; thus, system 5 of Table 6 includes formation of the trimethylindium adduct with ammonia and System 6 with trimethylamine. In both cases we have assumed a 1:1 initial ratio for the two respective precursors. Our results indicate that for both adducts at 298 K there are equal amounts of $InCH_3$ and free ammonia or trimethylamine that are about 10 times smaller than the adduct concentration. Bradley et al.[35] indicated that at room temperature the adduct generated sufficient pressure to obtain an adduct spectrum with no trace of peaks from trimethylindium or trimethylamine, thus completely associated at room temperature. At 1000K, there seems to be no adduct, and the system becomes identical to system 3.

Indium Compounds with group V Elements. Group III−V materials may be used in fast microelectronic devices, since they are faster than conventional Si-type semiconductor materials. We have performed calculation on the following group V series: indium nitride, phosphide, arsenide, and antimonide (InN, InP, InAs, and InSb, respectively), as well as on the InN dimer (In_2N_2).

InN may be used for fabricating highly efficient light-emitting diodes,[73] solar cells,[74] optical coatings, and sensors.[75] The transport characteristics of InN are superior to those of GaN and GaAs, a distinct advantage in high-frequency centimeter and millimeter wave devices.[76] The InN versus In plus N_2 stability was studied using ultrahigh-pressure X-ray measurements by Krukowski et al.[5] InN is extremely difficult to synthesize because it is metastable up to 900 K at 1 atm. At higher temperatures it decomposes preferably to liquid In and N_2, it melts at 2146 K with an equilibrium N_2 pressure higher than 60 kbar, and the decomposition at temperatures below 930 K is believed to be kinetically controlled.[5] The specific heat of InN was found to be at 300 K 39.80 J mol^{-1} K^{-1} by Krukowski et al.[5] and 42.03 J mol^{-1} K^{-1} by Slack et al.[77] The difference is probably due to impurities of the InN crystals in the latter. (We obtained a heat capacity of 34.3 J mol^{-1} K^{-1} for gaseous InN at 300 K.) The decomposition of InN was also measured in a vacuum by heating a sample and recording partial pressure of the relevant gases;[2] decomposition occurs at much lower temperatures than its melting point and has an effective activation energy of 336 kJ mol^{-1}. This activation energy is a factor of 1.5 to 1.9 higher than the binding energy of a single In−N bond (about 165 kJ mol^{-1} from Table 5, reaction 24; an experimental value[78] of 186 kJ mol^{-1}). By ion-assisted molecular beam epitaxy, the maximum deposition temperatures for the growth of InN were found to be between 1060 and 1130 K.[2]

Despite the experimental difficulties, InN has been prepared on Si(100) by laser-assisted chemical vapor deposition from low-pressure HN_3 and trimethylindium.[79] InN has been grown by epitaxy on sapphire.[80−82] On the other hand, InP is easier to obtain. InP layers were grown by hydride vapor phase epitaxy by McCollum et al.[83] The first preparation of InP using flow modulation techniques in the hydride vapor phase epitaxial system was done by Wang et al.[84] Highly pure InP layers were obtained from trimethylindium and phosphine in H_2 at 900 K by chemical beam epitaxy[85] and by atmospheric pressure OMCVD.[86] A procedure to grow InP from trimethylindium and phosphine in H_2 and N_2 at atmospheric pressures and 920 K was obtained by Sacilotti et al.[87] With respect to other indium-group V materials, InAs layers were grown using atomic layer epitaxy from indium chlorides and arsenic hydride by Kattelus et al.[88] and using OMCVD from arsine and trimethylindium by Partin et al.[89] InSb, used as magnetic position sensors in automobiles, has been grown also by OMCVD by Partin et al.[90] and Egan et al.[91]

The calculations of Balasubramanian et al.[38] resulted in a $^3\Sigma^-$ state for InSb, with a bond distance of 3.02 Å, a vibrational frequency of 121 cm^{-1}, and a D_e of 135 kJ mol^{-1} (4% smaller

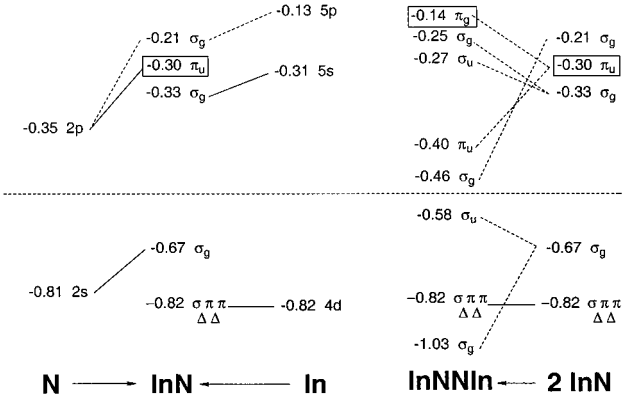

Figure 5. Molecular orbital diagram of indium nitride and indium nitride dimer (energy units: hartree).

than the reported experimental[37] value of 141 kJ mol^{-1}). These calculations were performed using relativistic effective core potentials, complete active space multiconfiguration self-consistent field, and multireference singles plus doubles configuration interaction. Calculations have been reported by Liao et al.[39] for the ^1A_g state of the indium antimonide dimer (In_2Sb_2), corresponding to a rhombus structure.

We did not obtain a stable calculation on singlet InN, which showed large singlet−triplet mixing. The stable structure found for InN and for the other group V compounds were $^3\Sigma^-$. The series InN, InP, InAs, and InSb shows the following increasing bond distances of (Table 3): 2.100, 2.696, 2.775, 2997 Å, respectively, and decreasing vibrational frequencies (Table 4) of 597,237,173 140 cm^{-1}, respectively. The 0 K dissociation enthalpies for the series were 160, 190, 181, and 166 kJ mol^{-1} (reactions 24 and 28−30, Table 5). The 0 K dissociation energy for InN with respect to In plus 0.5 N_2 at standard pressure conditions (reaction 25, Table 5) was determined as −304 kJ mol^{-1}. The molecular orbital diagram for this molecule (Figure 5) shows an In−N bonding orbital of higher energy that the singly occupied π orbitals on the N atom.

Two structures of the InN dimer were obtained: a linear $^3\Sigma_g$ molecule with the two nitrogen atoms bonded, and a ^1A_g rhombic molecule. The linear structure was found to be lower in energy by only 2 kJ mol^{-1} (0.0008 hartree; see Table 2). The In−N bond distances in the linear structure was 7% smaller than in the rhombus, and the N−N distance was 5% less (Table 3). The dissociation energy of the linear molecule at 0 K was calculated to be 673 kJ mol^{-1} (reaction 26, Table 5) with respect to two InN, but only 66 kJ mol^{-1} (reaction 27, Table 5) with respect to two In atoms and N_2. Figure 5 depicts the dramatic drop in energy that the bonding orbital from a single InN (σ_g) molecule undergoes in forming the dimer. For the latter, the open shell orbitals are the highest in energy (π_g).

System 7 of Table 6 contains the dimerization of indium nitride at 1000 K and 1 atm, with its dissociation into In and N_2, and possible formation of In_2 and In_3. The equilibrium composition results in 97% of In as In_3, 2% as In_2, less than 1% as In atom, and no dimer.

Concluding Remarks

We have shown that DFT is an adequate method for performing calculations on indium compounds. Our results showed that energies of molecules for which experimental data is available could be calculated within a few kiloJoules and frequencies within 10%. Thus, the thermodynamic properties derived from using the DFT calculations can be used in OMCVD modeling. In this respect, we have generated a consistent set of data to calculate the thermodynamic properties between 300 and 5000K for the following indium compounds: InF, InCl, $InCl_3$, InH, InH_2, InH_3, In_2, In_3, $In(CH_3)$, $In(CH_3)H$, $In(CH_3)H_2$, $In(CH_3)_2$, $In(CH_3)_2H$, $In_2(CH_3)_4$, $In(CH_3)_3$, $In(CH_3)_2$-CH_2, $In(CH_3)CH_2$, $In(CH_2)$, $(CH_3)_3In{:}NH_3$, $(CH_3)_3In{:}N(CH_3)_3$, $In(CH_3)_2(NH_2)$, $In(CH_3)(NH)$, InN, In_2N_2, InP, InAs, and InSb.

For a system in equilibrium at 1000 K, when In atoms are produced in the absence of other species such as H, In_3 will be the main species present with 97%. The amount of indium present as In_2 will be 2.4%, and as In atoms 0.5%.

On the other hand, when In and H_2 are initially in a 1:1 ratio, and only the indium hydrides are considered (no In cluster formation), InH is the predominant species at 298 K. At 1000K, InH and In atoms would be found at a ratio of 5:1.

In an equilibrium system at 1000 K that initially contains only trimethylindium, one expects about a third of the indium to be as In_3 (38%), and the hydrocarbon to be C_2H_6 (no CH_4 nor H_2). The other important indium species would be $In(CH_2)$ (37%), In_2 (2%) and less than 1% as $In(CH_3)$ and In atoms.

When a simplified trimethylindium dissociation is considered in the presence of ammonia or trimethylamine, our equilibrium calculations show equal amounts of $InCH_3$ and free ammonia or trimethylamine, 10 times smaller than the adduct concentration at room temperature. At 1000 K we expect no adduct formation.

The indium nitride molecule was found to be thermodynamically unstable with respect to indium atom and molecular nitrogen at any temperature considered and 1 atm. Nevertheless, a linear indium nitride dimer could form in the gas phase that could be stable with respect to two indium atoms and molecular nitrogen by as much as 69 kJ mol^{-1} at room temperature (63 kJ mol^{-1} at 1000 K). However, when formation of indium clusters is considered at 1000 K and 1 atm, all dimers would dissociate to form mainly In_3 (97%), and small amounts of In_2 (2%).

Acknowledgment. The work reported in this paper has been possible through the partial support provided by NASA (Cooperative Agreements NCC8-95, NCC8-194, and NCC8-144; and Grant NAG5-6532) and NSF (Grant HRD9450386). One of the authors (Carlos Cardelino) wishes to acknowledge NASA's Visiting Fellowship Program for his 1998 and 1999 summer work at Marshall Space Flight Center.

Appendix 1

Calculations for Table 8 are based on electronic and vibrational energies obtained using DFT theory.

The coefficients z_1-z_7 satisfy the following equations for Kelvin temperatures:

$$C_p/R = z_1 + z_2T + z_3T^2 + z_4T^3 + z_5T^4$$

$$H/R = z_1T + (z_2/2)T^2 + (z_3/3)T^3 + (z_4/4)T^4 + (z_5/5)T^5 + z_6$$

$$S/R = z_1 \ln T + z_2T + (z_3/2)T^2 + (z_4/3)T^3 + (z_5/4)T^4 + z_7$$

Values are provided for two temperature ranges: 300−1000 K (low) and 1000−5000 K (high).

TABLE 8: JANAF-Type Coefficients to Calculate Thermodynamic Properties of Indium Species as a Function of Temperature

species	temperature range	z_1	z_2	z_3	z_4	z_5	z_6	z_7
InF	low	3.276689	3.642293×10^{-03}	$-4.159896 \times 10^{-06}$	2.077002×10^{-09}	$-3.789125 \times 10^{-13}$	$-1.843683 \times 10^{+09}$	8.829404
	high	4.330501	1.771601×10^{-04}	$-7.048899 \times 10^{-08}$	1.219680×10^{-11}	$-7.676527 \times 10^{-16}$	$-1.843683 \times 10^{+09}$	3.564662
InCl	low	3.423117	4.496811×10^{-03}	$-6.529388 \times 10^{-06}$	3.891661×10^{-09}	$-8.130438 \times 10^{-13}$	$-1.957480 \times 10^{+09}$	9.329684
	high	4.447954	5.471581×10^{-05}	$-2.184676 \times 10^{-08}$	3.788755×10^{-12}	$-2.388328 \times 10^{-16}$	$-1.957480 \times 10^{+09}$	4.527942
$InCl_3$	low	5.146275	2.072796×10^{-02}	$-3.062453 \times 10^{-05}$	1.848707×10^{-08}	$-3.899157 \times 10^{-12}$	$-2.248158 \times 10^{+09}$	7.057404
	high	9.757765	2.543969×10^{-04}	$-1.015114 \times 10^{-07}$	1.759741×10^{-11}	$-1.108984 \times 10^{-15}$	$-2.248159 \times 10^{+09}$	$-1.442838 \times 10^{+01}$
In doublet	low	2.500000	2.264855×10^{-14}	$-5.811324 \times 10^{-17}$	4.235165×10^{-20}	$-9.926167 \times 10^{-24}$	$-1.812120 \times 10^{+09}$	6.643340
	high	2.500000	1.243450×10^{-14}	$-7.806256 \times 10^{-18}$	1.905824×10^{-21}	$-1.033976 \times 10^{-25}$	$-1.812120 \times 10^{+09}$	6.643340
In quartet	low	2.500000	2.264855×10^{-14}	$-5.811324 \times 10^{-17}$	4.235165×10^{-20}	$-9.926167 \times 10^{-24}$	$-1.812072 \times 10^{+09}$	7.336487
	high	2.500000	1.243450×10^{-14}	$-7.806256 \times 10^{-18}$	1.905824×10^{-21}	$-1.033976 \times 10^{-25}$	$-1.812072 \times 10^{+09}$	7.350301
In_2 triplet	low	3.927053	2.949142×10^{-03}	$-4.790919 \times 10^{-06}$	3.057664×10^{-09}	$-6.685872 \times 10^{-13}$	$-3.624255 \times 10^{+09}$	$1.002761 \times 10^{+01}$
	high	4.493317	7.041198×10^{-06}	$-2.814981 \times 10^{-09}$	4.885896×10^{-13}	$-3.081690 \times 10^{-17}$	$-3.624255 \times 10^{+09}$	7.509656
In_2 quintet	low	3.602690	4.174574×10^{-03}	$-6.437893 \times 10^{-06}$	3.983282×10^{-09}	$-8.533805 \times 10^{-13}$	$-3.624226 \times 10^{+09}$	1.118053×10^{01}
	high	4.475872	2.539903×10^{-05}	$-1.014927 \times 10^{-08}$	1.761030×10^{-12}	$-1.110497 \times 10^{-16}$	$-3.624226 \times 10^{+09}$	7.192563
In_3	low	5.494068	7.705298×10^{-03}	$-1.248267 \times 10^{-05}$	7.954317×10^{-09}	$-1.737579 \times 10^{-12}$	$-5.436393 \times 10^{+09}$	$1.139327 \times 10^{+01}$
	high	6.980864	2.015876×10^{-05}	$-8.058771 \times 10^{-09}$	1.398692×10^{-12}	$-8.821781 \times 10^{-17}$	-5.436393×10	4.773782
InH	low	3.478754	$-2.131544 \times 10^{-04}$	2.494571×10^{-06}	$-2.022239 \times 10^{-09}$	4.756463×10^{-13}	$-1.812310 \times 10^{+09}$	5.130985
	high	3.606693	8.873111×10^{-04}	$-3.421729 \times 10^{-07}$	5.800371×10^{-11}	$-3.599099 \times 10^{-15}$	$-1.812310 \times 10^{+09}$	3.998166
InH_2	low	3.797204	2.249223×10^{-03}	2.053784×10^{-06}	$-2.524677 \times 10^{-09}$	6.582394×10^{-13}	$-1.812486 \times 10^{+09}$	6.581640
	high	4.669357	2.286217×10^{-03}	$-8.747902 \times 10^{-07}$	1.475302×10^{-10}	$-9.121521 \times 10^{-15}$	$-1.812486 \times 10^{+09}$	1.274295
InH_3	low	3.401592	8.066662×10^{-03}	$-2.219764 \times 10^{-06}$	$-1.080839 \times 10^{-09}$	4.791638×10^{-13}	$-1.812680 \times 10^{+09}$	5.975110
	high	5.913395	3.982040×10^{-03}	$-1.517394 \times 10^{-06}$	2.552103×10^{-10}	$-1.574964 \times 10^{-14}$	$-1.812681 \times 10^{+09}$	-7.943076
$InCH_3$	low	3.362128	1.094972×10^{-02}	$-5.961956 \times 10^{-06}$	1.703911×10^{-09}	$-2.030469 \times 10^{-13}$	$-1.824722 \times 10^{+09}$	9.020252
	high	5.142802	6.684412×10^{-03}	$-2.329048 \times 10^{-06}$	3.685072×10^{-10}	$-2.177773 \times 10^{-14}$	$-1.824723 \times 10^{+09}$	$-4.185757 \times 10^{-01}$
$InCH_2$	low	3.474743	1.191599×10^{-02}	$-1.279330 \times 10^{-05}$	6.917552×10^{-09}	$-1.395598 \times 10^{-12}$	$-1.824515 \times 10^{+09}$	9.899514
	high	5.521158	3.684277×10^{-03}	$-1.251361 \times 10^{-06}$	1.942307×10^{-10}	$-1.131256 \times 10^{-14}$	$-1.824516 \times 10^{+09}$	1.181749×10^{-01}
$In(CH_3)H$	low	4.545518	1.390159×10^{-02}	$-6.897573 \times 10^{-06}$	1.384459×10^{-09}	$-4.107036 \times 10^{-14}$	$-1.824898 \times 10^{+09}$	5.504429
	high	7.313344	7.945662×10^{-03}	$-2.803228 \times 10^{-06}$	4.476747×10^{-10}	$-2.664226 \times 10^{-14}$	$-1.824899 \times 10^{+09}$	$-1.108731 \times 10^{+01}$
$In(CH_3)H_2$	low	4.130454	2.002846×10^{-02}	$-1.178356 \times 10^{-05}$	3.267505×10^{-09}	$-3.245167 \times 10^{-13}$	$-1.825091 \times 10^{+09}$	6.567218
	high	8.594697	9.623867×10^{-03}	$-3.443492 \times 10^{-06}$	5.554406×10^{-10}	$-3.329603 \times 10^{-14}$	$-1.825093 \times 10^{+09}$	$-1.886796 \times 10^{+01}$
$In(CH_3)_2$	low	5.789203	2.367515×10^{-02}	$-1.340860 \times 10^{-05}$	3.975850×10^{-09}	$-4.869591 \times 10^{-13}$	$-1.837310 \times 10^{+09}$	1.832245
	high	9.940690	1.362595×10^{-02}	$-4.740298 \times 10^{-06}$	7.493159×10^{-10}	$-4.425633 \times 10^{-14}$	$-1.837311 \times 10^{+09}$	$-2.356157 \times 10^{+01}$
$In(CH_3)(CH_2)$	low	5.105322	2.716529×10^{-02}	$-2.324470 \times 10^{-05}$	1.073922×10^{-08}	$-1.969912 \times 10^{-12}$	$-1.837101 \times 10^{+09}$	7.500612
	high	$1.023562 \times 10^{+01}$	1.071877×10^{-02}	$-3.700818 \times 10^{-06}$	5.817763×10^{-10}	$-3.422027 \times 10^{-14}$	$-1.837102 \times 10^{+09}$	$-2.095709 \times 10^{+01}$
$In_2(CH_3)_4$	low	$1.047716 \times 10^{+01}$	6.331793×10^{-02}	$-5.181944 \times 10^{-05}$	2.376792×10^{-08}	$-4.428832 \times 10^{-12}$	$-3.674643 \times 10^{+09}$	-3.772240
	high	$2.190128 \times 10^{+01}$	2.776387×10^{-02}	$-9.685255 \times 10^{-06}$	1.534046×10^{-09}	$-9.073853 \times 10^{-14}$	$-3.674647 \times 10^{+09}$	$-7.085783 \times 10^{+01}$
$In(CH3)_2H$	low	3.561245	2.623477×10^{-02}	$-3.837975 \times 10^{-06}$	$-5.471097 \times 10^{-09}$	1.885071×10^{-12}	$-1.837498 \times 10^{+09}$	$1.059061 \times 10^{+01}$
	high	$1.034382 \times 10^{+01}$	1.744112×10^{-02}	$-6.475599 \times 10^{-06}$	1.070588×10^{-09}	$-6.528628 \times 10^{-14}$	$-1.837500 \times 10^{+09}$	$-3.060567 \times 10^{+01}$
$In(CH_3)_3$	low	7.284643	3.750540×10^{-02}	$-2.237466 \times 10^{-05}$	7.243933×10^{-09}	$-1.002637 \times 10^{-12}$	$-1.849915 \times 10^{+09}$	-4.488778
	high	$1.395932 \times 10^{+01}$	2.090304×10^{-02}	$-7.292570 \times 10^{-06}$	1.155158×10^{-09}	$-6.833166 \times 10^{-14}$	$-1.849915 \times 10^{+09}$	$-4.483178 \times 10^{+01}$
$In(CH_3)_2(CH_2)$	low	6.676739	4.135231×10^{-02}	$-3.317179 \times 10^{-05}$	1.471743×10^{-08}	$-2.650844 \times 10^{-12}$	$-1.849707 \times 10^{+09}$	1.297272
	high	$1.434668 \times 10^{+01}$	1.788989×10^{-02}	$-6.209295 \times 10^{-06}$	9.799007×10^{-10}	$-5.780509 \times 10^{-14}$	$-1.849709 \times 10^{+09}$	$-4.214114 \times 10^{+01}$
$In(CH_3)_3NH_3$	low	8.467926	5.936325×10^{-02}	$-4.873854 \times 10^{-05}$	2.276396×10^{-08}	$-4.311500 \times 10^{-12}$	$-1.867777 \times 10^{+09}$	-8.177523
	high	$1.845289 \times 10^{+01}$	2.716972×10^{-02}	$-9.347440 \times 10^{-06}$	1.466190×10^{-09}	$-8.611813 \times 10^{-14}$	$-1.867780 \times 10^{+09}$	$-6.534638 \times 10^{+01}$
$In(CH_3)_2NH_2$	low	6.595007	4.189039×10^{-02}	$-3.483474 \times 10^{-05}$	1.597016×10^{-08}	$-2.937211 \times 10^{-12}$	$-1.854989 \times 10^{+09}$	7.498049×10^{-01}
	high	$1.424858 \times 10^{+01}$	1.760149×10^{-02}	$-6.022486 \times 10^{-06}$	9.410117×10^{-10}	$-5.511733 \times 10^{-14}$	$-1.854989 \times 10^{+09}$	$-4.196310 \times 10^{+01}$
$In(CH_3)NH$	low	5.080469	2.188062×10^{-02}	$-1.757335 \times 10^{-05}$	7.600917×10^{-09}	$-1.320608 \times 10^{-12}$	$-1.842185 \times 10^{+09}$	3.031273
	high	9.440717	8.795933×10^{-03}	$-3.021779 \times 10^{-06}$	4.735161×10^{-10}	$-2.779352 \times 10^{-14}$	$-1.842186 \times 10^{+09}$	$-2.273476 \times 10^{+01}$
$In(CH_3)_3N(CH_3)_3$	low	9.465587	8.726367×10^{-02}	$-5.488191 \times 10^{-05}$	1.927767×10^{-08}	$-2.960246 \times 10^{-12}$	$-1.904994 \times 10^{+09}$	$-1.215876 \times 10^{+01}$
	high	$2.564312 \times 10^{+01}$	4.661636×10^{-02}	$-1.645350 \times 10^{-05}$	2.628333×10^{-09}	$-1.564462 \times 10^{-13}$	$-1.905000 \times 10^{+09}$	$-1.092736 \times 10^{+02}$
$In(CH_3)_3N(H_2)$-$N(H_2)$	low	8.249625	6.665694×10^{-02}	$-5.142962 \times 10^{-05}$	2.252312×10^{-08}	$-4.075728 \times 10^{-12}$	$-1.885241 \times 10^{+09}$	-2.497257
	high	$2.021396 \times 10^{+01}$	3.091491×10^{-02}	$-1.069146 \times 10^{-05}$	1.683663×10^{-09}	$-9.919145 \times 10^{-14}$	$-1.885244 \times 10^{+09}$	$-6.983439 \times 10^{+01}$
InN	low	3.283073	3.882000×10^{-03}	$-4.696143 \times 10^{-06}$	2.459678×10^{-09}	$-4.670922 \times 10^{-13}$	$-1.829380 \times 10^{+09}$	9.643050
	high	4.356156	1.505430×10^{-04}	$-5.994575 \times 10^{-08}$	1.037780×10^{-11}	$-6.533974 \times 10^{-16}$	$-1.829381 \times 10^{+09}$	4.343562
In_2N_2linear	low	4.835566	1.993781×10^{-02}	$-2.806321 \times 10^{-05}$	1.677836×10^{-08}	$-3.542116 \times 10^{-12}$	$-3.658841 \times 10^{+09}$	8.121772
	high	9.153831	1.315658×10^{-03}	$-5.023160 \times 10^{-07}$	8.459542×10^{-11}	$-5.225438 \times 10^{-15}$	$-3.658842 \times 10^{+09}$	$-1.220324 \times 10^{+01}$
InP	low	3.527725	4.360892×10^{-03}	$-6.593534 \times 10^{-06}$	4.030634×10^{-09}	$-8.566094 \times 10^{-13}$	$-1.919910 \times 10^{+09}$	$1.009607 \times 10^{+01}$
	high	4.467333	3.437475×10^{-05}	$-1.373260 \times 10^{-08}$	2.382414×10^{-12}	$-1.502177 \times 10^{-16}$	$-1.919910 \times 10^{+09}$	5.766022
InAs	low	3.686201	3.912145×10^{-03}	$-6.138162 \times 10^{-06}$	3.837508×10^{-09}	$-8.278213 \times 10^{-13}$	$-2.518157 \times 10^{+09}$	$1.066779 \times 10^{+01}$
	high	4.482586	1.833778×10^{-05}	$-7.329021 \times 10^{-09}$	1.271835×10^{-12}	$-8.020801 \times 10^{-17}$	$-2.518157 \times 10^{+09}$	7.060861
InSb	low	3.793803	3.512985×10^{-03}	$-5.609680 \times 10^{-06}$	3.544067×10^{-09}	$-7.698108 \times 10^{-13}$	$-3.805214 \times 10^{+09}$	$1.110189 \times 10^{+01}$
	high	4.488541	1.207020×10^{-05}	$-4.824873 \times 10^{-09}$	8.373699×10^{-13}	$-5.281246 \times 10^{-17}$	$-3.805214 \times 10^{+09}$	7.983709
other species								
H	low	2.500000	2.264855×10^{-14}	$-5.811324 \times 10^{-17}$	4.235165×10^{-20}	$-9.926167 \times 10^{-24}$	$-1.585674 \times 10^{+05}$	$-4.600092 \times 10^{-01}$
	high	2.500000	1.243450×10^{-14}	$-7.806256 \times 10^{-18}$	1.905824×10^{-21}	$-1.033976 \times 10^{-25}$	$-1.585674 \times 10^{+05}$	$-4.600092 \times 10^{-01}$
H_2	low	3.500422	3.312113×10^{-05}	$-2.478260 \times 10^{-07}$	4.011975×10^{-10}	$-1.148223 \times 10^{-13}$	$-3.692977 \times 10^{+05}$	-4.275289
	high	3.062400	5.615640×10^{-04}	$-4.574501 \times 10^{-08}$	$-8.712460 \times 10^{-12}$	1.173360×10^{-15}	$-3.691168 \times 10^{+05}$	-1.775952
Cl	low	2.500000	2.264855×10^{-14}	$-5.811324 \times 10^{-17}$	4.235165×10^{-20}	$-9.926167 \times 10^{-24}$	$-1.453081 \times 10^{+08}$	4.880603
	high	2.500000	1.243450×10^{-14}	$-7.806256 \times 10^{-18}$	1.905824×10^{-21}	$-1.033976 \times 10^{-25}$	$-1.453081 \times 10^{+08}$	4.880603
Cl_2	low	3.282660	3.871732×10^{-03}	$-4.672593 \times 10^{-06}$	2.442704×10^{-09}	$-4.631583 \times 10^{-13}$	$-2.906391 \times 10^{+08}$	7.267773
	high	4.355052	1.516902×10^{-04}	$-6.040054 \times 10^{-08}$	1.045630×10^{-11}	$-6.583303 \times 10^{-16}$	$-2.906393 \times 10^{+08}$	1.968984

TABLE 8 (Continued)

species	temperature range	z_1	z_2	z_3	z_4	z_5	z_6	z_7
CH_3	low	3.810641	2.657614×10^{-03}	2.018941×10^{-06}	$-1.837437 \times 10^{-09}$	3.938933×10^{-13}	$-1.257541 \times 10^{+07}$	2.643879
	high	3.108591	5.504099×10^{-03}	$-1.828297 \times 10^{-06}$	2.790690×10^{-10}	$-1.604823 \times 10^{-14}$	$-1.257529 \times 10^{+07}$	5.973501
CH_4	low	4.000979	$-2.294438 \times 10^{-03}$	1.522343×10^{-05}	$-1.073612 \times 10^{-08}$	2.313520×10^{-12}	$-1.278539 \times 10^{+07}$	$-3.278980 \times 10^{-01}$
	high	1.880234	9.406498×10^{-03}	$-3.264305 \times 10^{-06}$	5.149882×10^{-10}	$-3.036938 \times 10^{-14}$	$-1.278527 \times 10^{+07}$	8.725102
C_2H_6	low	3.879388	6.552222×10^{-03}	1.584851×10^{-05}	$-1.430140 \times 10^{-08}$	3.385888×10^{-12}	$-2.519272 \times 10^{+07}$	3.949507
	high	4.228544	1.583996×10^{-02}	$-5.596418 \times 10^{-06}$	8.945776×10^{-10}	$-5.327179 \times 10^{-14}$	$-2.519384 \times 10^{+07}$	-2.867215
N	low	2.500000	2.264855×10^{-14}	$-5.811324 \times 10^{-17}$	4.235165×10^{-20}	$-9.926167 \times 10^{-24}$	$-1.724076 \times 10^{+07}$	4.180742
	high	2.500000	1.243450×10^{-14}	$-7.806256 \times 10^{-18}$	1.905824×10^{-21}	$-1.033976 \times 10^{-25}$	$-1.724076 \times 10^{+07}$	4.180742
N_2	low	3.548647	$-6.838606 \times 10^{-04}$	1.887261×10^{-06}	$-1.060433 \times 10^{-09}$	1.892244×10^{-13}	$-3.459307 \times 10^{+07}$	2.929300
	high	2.943360	1.357266×10^{-03}	$-4.797248 \times 10^{-07}$	7.656062×10^{-11}	$-4.549143 \times 10^{-15}$	$-3.459294 \times 10^{+07}$	5.923834
NH_3	low	4.230241	2.676514×10^{-02}	4.451251×10^{-06}	$-1.130801 \times 10^{-08}$	3.100456×10^{-12}	$-5.507075 \times 10^{+07}$	8.842416
	high	9.203082	2.583654×10^{-02}	$-9.237978 \times 10^{-06}$	1.489194×10^{-09}	$-8.922561 \times 10^{-14}$	$-5.507423 \times 10^{+07}$	$-2.695403 \times 10^{+01}$
$N(CH_3)_3$	low	4.230241	2.676514×10^{-02}	4.451251×10^{-06}	$-1.130801 \times 10^{-08}$	3.100456×10^{-12}	$-5.507237 \times 10^{+07}$	$1.756411 \times 10^{+01}$
	high	9.203082	2.583654×10^{-02}	$-9.237978 \times 10^{-06}$	1.489194×10^{-09}	$-8.922561 \times 10^{-14}$	$-5.507479 \times 10^{+07}$	-9.766706
N_2H_4	low	3.904113	6.360109×10^{-03}	6.337039×10^{-06}	$-6.801982 \times 10^{-09}$	1.691703×10^{-12}	$-3.531756 \times 10^{+07}$	7.036976
	high	4.539046	9.688597×10^{-03}	$-3.265477 \times 10^{-06}$	5.049879×10^{-10}	$-2.936402 \times 10^{-14}$	$-3.531443 \times 10^{+07}$	1.947182
P	low	2.500000	2.264855×10^{-14}	$-5.811324 \times 10^{-17}$	4.235165×10^{-20}	$-9.926167 \times 10^{-24}$	$-1.077672 \times 10^{+08}$	5.371149
	high	2.500000	1.243450×10^{-14}	$-7.806256 \times 10^{-18}$	1.905824×10^{-21}	$-1.033976 \times 10^{-25}$	$-1.077672 \times 10^{+08}$	5.371149
As	low	2.500000	2.264855×10^{-14}	$-5.811324 \times 10^{-17}$	4.235165×10^{-20}	$-9.926167 \times 10^{-24}$	$-7.060152 \times 10^{+08}$	6.696102
	high	2.500000	1.243450×10^{-14}	$-7.806256 \times 10^{-18}$	1.905824×10^{-21}	$-1.033976 \times 10^{-25}$	$-7.060152 \times 10^{+08}$	6.696102
Sb	low	2.500000	2.264855×10^{-14}	$-5.811324 \times 10^{-17}$	4.235165×10^{-20}	$-9.926167 \times 10^{-24}$	$-1.993074 \times 10^{+09}$	7.424393
	high	2.500000	1.243450×10^{-14}	$-7.806256 \times 10^{-18}$	1.905824×10^{-21}	$-1.033976 \times 10^{-25}$	$-1.993074 \times 10^{+09}$	7.424393
F	low	2.500000	2.264855×10^{-14}	$-5.811324 \times 10^{-17}$	4.235165×10^{-20}	$-9.926167 \times 10^{-24}$	$-3.149958 \times 10^{+07}$	3.944824
	high	2.500000	1.243450×10^{-14}	$-7.806256 \times 10^{-18}$	1.905824×10^{-21}	$-1.033976 \times 10^{-25}$	$-3.149958 \times 10^{+07}$	3.944824

References and Notes

(1) Bachmann, K. J.; Cardelino, B. H.; Moore, C. E.; Cardelino, C. A.; Sukidi, N.; McCall, S. In *In Situ Process Diagnostics and Modeling*; Ochello, A., Krauss, A. R., Irene, E. A., Schultz, J. A., Eds.; Materials Research Society Symposium Proceedings; Materials Research Society: Warrendale, PA, 1999; Vol. 569, p 59.

(2) Ambacher, O.; Brandt, M. S.; Dimitrov, R.; Metzger, T.; Stutzmann, M.; Fischer, R. A.; Miehr, A.; Bergmaier, A.; Dollinger, G. *J. Vac. Sci. Technol. B* **1966**, *14*, 353.

(3) Bedair, S. M.; McIntosh, F. G.; Roberts, J. C.; Piner, E. L.; Boutros, K. S.; El-Masry, N. A. *J. Cryst. Growth* **1997**, *178*, 32.

(4) Bachmann, K.; McCall, S.; LeSure, S.; Sukidi, N.; Wang, F.; *Journal of the Japanese Society of Microgravity Applications* **1998**, *15*, 436.

(5) Krukowski, S.; Witek, A.; Adamczyk, J.; Jun, J.; Bockowski, M.; Grzegory, I.; Lucznik, B.; Nowak, G.; Wroblewski, M.; Presz, A.; Gierlotka, S.; Stelmach, S.; Palosz, B.; Porowski, S.; Zinn, P.; *J. Phys. Chem. Solids* **1998**, *59*, 289.

(6) Bachman, K. J.; Kepler, G. M. *SPIE* **1997**, *3123*, 64.

(7) Cardelino, C. A.; Moore, C. E.; Cardelino, B. H.; Zhou, N.; Lowry, S.; Krishnan, A.; Frazier, D. O.; Bachmann, K. J. *SPIE* **1999**, *3625*, 447.

(8) Usui, A.; Sunakawa, H.; Sakai, A.; Yamaguchi, A. *Jpn. J. Appl. Phys.* **1997**, *36*, L899.

(9) Dechtprom, T.; Hiramatsu, K.; Amano, H.; Akasaki, I. *Appl. Phys. Lett.* **1992**, *61*, 2688.

(10) Hasegawa, F.; Minami, M.; Sunaba, K.; Suematsu, T. *Jpn. J. Appl. Phys.* **1999**, *38*, L700.

(11) Pullumbi, P.; Mijoule, C.; Manceron, L.; Bouteiller, Y. *Chem. Phys.* **1994**, *185*, 13.

(12) Pullumbi, P.; Bouteiller, Y.; Manceron, L.; Mijoule, C. *Chem. Phys.* **1994**, *185*, 25.

(13) Leininger, T.; Nicklass, A.; Stoll, H.; Dolg, M.; Schwerdtfeger, P. *J. Chem. Phys.* **1996**, *105*, 1052.

(14) Bauschlicher, C. W., Jr. *Chem. Phys. Lett.* **1999**, *305*, 446.

(15) Schwerdtfeger, P.; Fischer, T.; Dolg, M.; Igel-Mann, G.; Nicklass, A.; Stoll, H.; Haarland, A. *J. Chem. Phys.* **1995**, *102*, 2050.

(16) Moncrieff, D.; Kobus, J. Wilson, S. *Mol. Phys.* **1998**, *93*, 713.

(17) Dobbs, K. D.; Hehre, W. J. *J. Computational Chemistry* **1986**, *7*, 359.

(18) Okamoto, Y. *J. Cryst. Growth* **1998**, *191*, 405.

(19) Huber, K. P.; Herzberg, G. *Molecular Spectra and Molecular Structure; Vol. IV, Constants of Diatomic Molecules*; Van Nostrand Reinhold: New York, 1979.

(20) Barin, I. *Thermochemical Data of Pure Substances*; VCH: Weinheim, 1993.

(21) Wagman, D. D.; Evans, W. H.; Parker, V. B.; Halow, I.; Bailey, S. M.; Schumm, R. H. Selected Values of Chemical Thermodynamic Properties. NBS Technical Note 270−3; National Bureau of Standards: Washington, DC, 1968.

(22) Vogt, N.; Haaland, A.; Martinsen, J.-G.; Vogt, J. *J. Mol. Spectrosc.* **1994**, *163*, 515.

(23) Teichteil, C.; Spiegelmann, F. *Chem. Phys.* **1983**, *81*, 283.

(24) Balasubramanian, K. *J. Phys. Chem.* **1990**, *94*, 6582.

(25) Balasubramanian, K.; Tao, J. X. *J. Chem. Phys.* **1991**, *94*, 3000.

(26) Bahnmaier, A. H.; Urban, R.-D.; Jones, H. *Chem. Phys. Lett.* **1989**, *155*, 269.

(27) White, J. B.; Dulick, M.; Bernath, P. F. *J. Mol. Spectrosc.* **1995**, *169*, 410.

(28) Rosen, B.; editor; *Spectroscopic Data Relative to Diatomic Molecules*; Pergamon Press: New York, 1970.

(29) Balducci, G.; Gigli, G.; Meloni, G. *J. Chem. Phys.* **1998**, *109*, 4384.

(30) Balasubramanian, K.; Li, J. *J. Chem. Phys.* **1988**, *88*, 4979.

(31) Feng, P. Y.; Balasubramanian, K. *Chem. Phys.* **1989**, *138*, 89.

(32) Igel-Mann, G.; Feller, C.; Flad, H.-J.; Savin, A.; Stoll, H.; Preuss, H. *Mol. Phys.* **1989**, *68*, 209.

(33) El-Nahas, A. M.; von Rague Schleyer, P. *J. Computational Chemistry* **1994**, *15*, 596.

(34) Buchan, N. I.; Larsen, C. A.; Stringfellow, G. B. *J. Cryst. Growth* **1988**, *92*, 605.

(35) Bradley, D. C.; Hamilton, P. A.; Harding, I. S.; Morton, N. W.; Rankin, D. W. H.; Robertson, H. E.; Vaghjiani, J. *Proc. R. Soc. London A* **1997**, *453*, 2123.

(36) Guo, Q. X.; Nishio, M.; Ogawa, H.; Wakahara, A.; Yoshida, A. *Phys. Rev. B* **1998**, *58*, 15404.

(37) Balasubramanian, K. *J. Chem. Phys.* **1990**, *93*, 507.

(38) Balasubramanian, K.; Tao, J. X.; Liao, D. W. *J. Chem. Phys.* **1991**, *95*, 4905.

(39) Liao, D. W.; Balasubramanian, K. *J. Chem. Phys.* **1992**, *96*, 8938.

(40) Frisch, M. J.; Trucks, G. W.; Schlegel, H. B.; Scuseria, G. E.; Robb, M. A.; Cheeseman, J. R.; Zakrzewski, V. G.; Montgomery, J. A., Jr.; Stratmann, R. E.; Burant, J. C.; Dapprich, S.; Millam, J. M.; Daniels, A. D.; Kudin, K. N.; Strain, M. C.; Farkas, O.; Tomasi, J.; Barone, V.; Cossi, M.; Cammi, R.; Mennucci, B.; Pomelli, C.; Adamo, C.; Clifford, S.; Ochterski, J.; Petersson, G. A.; Ayala, P. Y.; Cui, Q.; Morokuma, K.; Malick, D. K.; Rabuck, A. D.; Raghavachari, K.; Foresman, J. B.; Cioslowski, J.; Ortiz, J. V.; Stefanov, B. B.; Liu, G.; Liashenko, A.; Piskorz, P.; Komaromi, I.; Gomperts, R.; Martin, R. L.; Fox, D. J.; Keith, T.; Al-Laham, M. A.; Peng, C. Y.; Nanayakkara, A.; Gonzalez, C.; Challacombe, M.; Gill, P. M. W.; Johnson, B. G.; Chen, W.; Wong, M. W.; Andres, J. L.; Head-Gordon, M.; Replogle, E. S.; Pople, J. A. *Gaussian 98*, Revision A.7; Gaussian, Inc.: Pittsburgh, PA, 1998.

(41) Becke, A. D. *J. Chem. Phys.* **1993**, *98*, 5648.

(42) Lee, C.; Yang, W.; Parr, R. G. *Phys. Rev. B* **1988**, *37*, 785.

(43) Miehlich, B.; Savin, A.; Stoll, H.; Preuss, H. *Chem. Phys. Lett.* **1989**, *157*, 200.

(44) Dobbs, K. D.; Hehre, W. J.; *J. Comput. Chem.* **1986**, *7*, 359.

(45) Dobbs, K. D.; Hehre, W. J. *J. Comput. Chem.* **1987**, *8*, 861.

(46) Dobbs, K. D.; Hehre; W. J. *J. Comput. Chem.* **1987**, *8*, 880.

(47) Provided by *Gaussian 98*, Revision A.7 [see ref 40], and identified as AKR and WAG 1982.
(48) Lucas, K. *Applied Statistical Thermodynamics*; Springer-Verlag: Berlin Heidelberg, 1991.
(49) Chase, M. W. *JANAF Thermochemical Tables*; American Chemical Society: Washington, DC, and American Institute of Physics: New York, for the National Bureau of Standards; issued as Supplement #1 to Volume 14 of the *Journal of Physical and Chemical Reference Data*; 3rd ed., 1986.
(50) *FORTRAN Program JANAF*. It can be requested from the corresponding author. The input to the program is an output file of a Gaussian98 geometry optimization and frequency calculation. The program allows for a multiplicative correction to the vibrational frequencies. Any pressure is accepted. Real gas treatment can be optionally achieved through a virial correction based on Lennard-Jones parameters, which are requested interactively during the run.
(51) Perdew, J. P. *Phys. Rev.* **1986**, *B33*, 8822.
(52) Perdew, J. P.; Wang, Y. *Phys Rev.* **1992**, *B45*, 244.
(53) Wong, M. W. *Chem. Phys. Lett.* **1996**, *256*, 391.
(54) Bauschlicher, C. W., Jr.; Partridge, H. *J. Chem. Phys.* **1995**, *103*, 1788.
(55) Thomas, J. R.; DeLeeuw, B. J.; Vacek, G.; Crawford, T. D.; Yamaguchi, Y.; Schaefer, H. F., III *J. Chem. Phys.* **1993**, *99*, 403.
(56) Hebner, G. A.; Killeen, K. P. *J. Appl. Phys.* **1990**, *67*, 1598.
(57) De Maria, G.; Drowart, J.; Inghram, M. G. *J. Chem. Phys.* **1959**, *31*, 1076.
(58) Drowart, J.; Honig, R. E. *J. Phys. Chem.* **1957**, *61*, 980.
(59) Gingerich, K. A.; Blue, G. D. Presentation at the 18th Annual Conference on Mass Spectrometry and Allied Topics, San Francisco, CA, 1970.
(60) Froben, F. W.; Schulze, W.; Kloss, U. *Chem. Phys. Lett.* **1983**, *99*, 500.
(61) Larsen, C. A.; Buchan, N. I.; Li, S. H.; Stringfellow, G. B. *J. Cryst. Growth* **1990**, *102*, 103.
(62) Jacko, M. G.; Price, S. J. W. *Can. J. Chem.* **1963**, *41*, 1460.
(63) Buchan, N. I.; Larsen, C. A.; Stringfellow, G. B. *Appl. Phys. Lett.* **1987**, *51*, 1024.
(64) Larsen, C. A.; Stringfellow, G. B. *J. Cryst. Growth* **1986**, *75*, 247.
(65) Shogen, S.; Ohashi, M.; Hashimoto, S.; Kawasaki, M.; Hosokawa, Y.; Atwater, H. A.; Chason, E.; Grabow, M. H.; Lagally, M. G. In *Evolution of Surface and Thin Film Microstructure, Symposium*; Atwater, H. A., Chason, E., Gravow, M. G., Lagally, M. G., Eds.; Materials Research Society: Pittsburgh, PA, 1993; p 193.
(66) Bu, Y.; Chu, J. C. S.; Shinn, D. W.; Lin, M. C. *Mater. Chem. and Phys.* **1993**, *33*, 99.
(67) Hebner, G. A.; Killeen, K. P. *J. Appl. Phys.* **1990**, *67*, 2598.
(68) Fan, G. H.; Hoare, R. D.; Pemble, M. E.; Povey, I. M.; Taylor, A. G.; Williams, J. O. *J. Cryst. Growth* **1992**, *124*, 49.
(69) Allendork, M. D.; McDaniel, A. H. In *Chemical Aspects of Electronic Ceramics Processing; Symposium*; Kumpta, P. N., Hepp, A. F., Beach, D. B., Arkles, B., Sullivan, J. J., Eds.; Materials Research Society: Warrendale, PA, 1998, p 125.
(70) Karlicek, R.; Long, J. A.; Donnelly, V. M. *J. Cryst. Growth* **1984**, *68*, 123.
(71) Cheng, C. H.; Jones, K. A. *J. Electron. Mater.* **1984**, *13*, 703.
(72) Larsen, C. A.; Buchan, N. I.; Stringfellow, G. B. *J. Cryst. Growth* **1987**, *85*, 148.
(73) Nakamura, S.; Mukai, T.; Senoh, M.; Iwasa, N.; *Jpn, J. Appl. Phys.* **1992**, *31*, 139.
(74) Neil, M. E.; Barnett, A. M. *IEEE Trans. Electron. Devices ED-34* **1987**, 257.
(75) Strite, S.; Morkof, H. *J. Vac. Sci. Technol. B* **1992**, *10*, 1237.
(76) O'Leary, S. K.; Foutz, B. E.; Shur, M. S.; Bhapkar, U. V.; Eastman, L. F. *J. Appl. Phys.* **1998**, *83*, 826.
(77) Slack, G. A.; Tanzili, R. A.; Pohl, R. O.; Vandersande, J. W. *J. Phys. Chem. Solids* **1987**, *48*, 641.
(78) Edgar, J. H. *Group III Nitrides*; INSPEC: London, 1994.
(79) Bu, Y.; Ma, L.; Lin, M. C. *J. Vac. Sci. Technol. A* **1993**, *11*, 2931.
(80) Wakahara, A.; Yoshida, A. *Appl. Phys. Lett.* **1989**, *54*, 709.
(81) Kistenmacher, T. J.; Bryden, W. A. *Appl. Phys. Lett.* **1991**, *59*, 1844.
(82) Igarashi, O. *Jpn, J. Appl. Phys. Part 1* **1992**, *31*, 2665.
(83) McCollum, M. J.; Kim, M. H.; Bose, S. S.; Lee, B.; Stillman, G. E. *Appl. Phys. Lett.* **1988**, *53*, 1868.
(84) Wang, P. J.; Wessels, B. W. *Appl. Phys. Lett.* **1986**, *49*, 564.
(85) Sudersena Rao, T.; Lacelle, C.; Roth, A. P. *J. Vac. Sci. Technol. B* **1993**, *11*, 840.
(86) Zilko, J. L.; Van Haren, D. L.; Lu, P. Y.; Shumaker, N. E.; Leung, S. Y. *J. Electron. Mater.* **1985**, *14*, 563.
(87) Sacilotti, M.; Mircea, A.; Azoulay, R. *J. Cryst. Growth* **1983**, *63*, 111.
(88) Kattelus, H. P.; Ahopelto, J.; Suni, I. *Acta Polytechnica Scandinavica, Electrical Engineering*; Series E164; Finnish Academy of Technical Sciences: Helsinki, 1989; p 155.
(89) Partin, D. L.; Green, L.; Morelli, D. T.; Heremans, J.; Fuller, B. K.; Thrush, C. M. *J. Electron. Mater.* **1991**, *20*, 1109.
(90) Partin, D. L.; Green, L.; Heremans, J. *J. Electron. Mater.* **1994**, *23*, 75.
(91) Egan, R. J.; Chin, V. W. L.; Tansley, T. L. *Semicond. Sci. Technol.* **1994**, *9*, 1491.